MONASH University

Enhanced Energy Absorption in Hierarchical Honeycomb Structures Using Foaming Materials: Design, Fabrication, and Characterization via Fused Filament Fabrication

Haoyang Yuan

Master of Engineering Science (Research)

A thesis submitted for the degree of Master at

Monash University in 2024

School of Engineering - Mechanical and Aerospace Engineering

Copyright Notice

Abstract

This thesis intestates the design, fabrication, and mechanical characterization of hierarchical honeycomb structures using foaming materials via Fused Filament Fabrication (FFF) process. Honeycomb structures are well known for their high strength-to-weight ratio and energy absorption. In this research, foaming PLA and solid PLA are added to overcome the weaknesses of conventional designs in mechanical performance and energy absorption capability.

A hierarchical design method is proposed in this thesis, considering micro-, meso-, and macroscale features to tailor relative density and mechanical properties. Foaming PLA materials were fabricated via FFF process with varying nozzle temperature $210°C, 230°C,$ and $250°C$ for porosity and mechanical performance control. Meanwhile, extrusion calibration ensured precision in dimensions and consistency in extrusion width. The mechanical test results showed that the foaming PLA printed at $250°C$ gave the highest specific modulus and energy absorption, hence providing great potential for energy absorption applications.

Hierarchical honeycomb structures with calibrated parameters were fabricated with foaming PLA as the core layer and solid PLA as the skin layer. In such a design, adjustable relative density with greatly enhanced stiffness and energy absorption performance was achieved. Tests results for compression demonstrated that the hierarchical structures outperformed the pure foaming PLA and solid PLA material. To further explain the experimental results, this research also employed numerical analysis tool, specifically finite element simulation, to analyze the differences in stress distribution between hierarchical honeycomb structures ($S_{max} = 7.4\ MPa,\ \sigma_{yield} = 35.43\ MPa$) and single-material honeycomb structures ($S_{max} = 2.0\ MPa,\ \sigma_{yield} = 2.71\ MPa$) to analyze load-bearing capacity. The finding evidence that the hierarchical designs combining foaming material are feasible to develop applications that require an innovative framework with superior energy absorption capability.

Declaration

This thesis is an original work of my research and contains no material which has been accepted for the award of any other degree or diploma at any university or equivalent institution and that, to the best of my knowledge and belief, this thesis contains no material previously published or written by another person, or any use of generative artificial intelligence technologies, except where due reference is made in the text of the thesis.

Signature:

Print Name: Haoyang Yuan

Date: 02/12/2024

Acknowledgement Part A

Over the past two years, great improvements have taken place, not only in academics but also in engineering practices and personal growth. This could not have been possible without the inspiring people I had the privilege of meeting on my journey.

First and foremost, I want to express deep thanks to my supervisor, Dr. Yunlong Tang. Throughout my studies, Dr. Yunlong provided invaluable support and guidance in my research while encouraging me during times of stress and challenges in graduate life. His timely and effective feedback, along with patient explanations, was instrumental in my progress. I am unable to imagine what I have achieved without his mentorship, and I truly believe he is the best supervisor one could ask for.

I would also like to express my deep appreciation to my co-supervisor, Professor Michael Yu Wang. Although he has left Monash University, his early involvement in my research gave me much guidance and inspiration.

Further to this, I would like to show great appreciation to every member of the Monash Centre for Additive Manufacturing (MCAM). The facilities and equipment for several rounds of experiments, along with the training and technical assistance they provided, were essential in my work.

Last but not least, I would like to express my special thanks to my parents, who have supported me financially and emotionally throughout this academic undertaking. Their encouragement freed me from any burden in pursuing the degree, while their soothing words lifted me up whenever I felt uncertain or vulnerable.

Acknowledgement Part B

I acknowledge the use of ChatGPT (https://chat.openai.com/) to refine the academic language and accuracy of my own work. I typed sentences with the instruction to “Polishing sentences in academic way”. I then selectively made further revisions to the results to better reflect my own writing tone and style.

Content

List of figures

List of tables

Chapter 1: Introduction

1.1 Cellular Materials

Advanced high-performance material development is required to create lightweight and strong structures, optimized for energy efficiency, and designed for sustainability [1]. Lightweight, highly strong engineering materials continue to be an especially difficult development problem. Given the challenge, researchers have turned to cellular materials that, in general, demonstrate excellent strength-to-weight ratio and unmatched energy absorption [2][3].

Cellular materials such as foams, honeycombs, and lattice structures generally have complex meso- or microscale architectures. These structures have remarkable advantages in macroscopic mechanical properties and open up new perspectives in engineering material design [4][5][6].

Cellular materials can modify their mechanical properties at the meso and microscale levels and, for this reason, play a very important role in many engineering applications. Modification of cell topology, size, and distribution enables the designer to adapt these materials to specific needs: from impact resistance to thermal insulation and noise reduction. Cellular materials, therefore, represent a flexible approach to attaining multi-functional performance and are hence a key focus in research in materials science and engineering.

1.2 Honeycomb Structures

Honeycomb structures bear several unique geometric configurations, in addition to anisotropic mechanical properties, and they are the cellular material that bears apt suitability for such wide applications like aerospace and automobile manufacturing, construction engineering. Another crucial characteristic of this material design is the flexibility provided by the latticework and what can be obtained by specific conformation change of a unit cell in a two-dimensional plane. Moreover, extending such geometries into three dimensions is a simplification in fabrication and additive manufacturing since the need for support structures is eliminated. With proper design and application of honeycomb architecture, material properties can be engineered to suit wide-ranging technical requirements, ensuring optimal performance [7].

1.3 Application of Honeycomb Structures

The design flexibility of honeycomb structures enables the tailoring of the mechanical properties for a host of applications, from implantable medical devices where the bio-compatible cellular materials might mirror the structures of native tissues to heat exchangers, whose geometries further assist in effective heat transport [8]. Applications continue to broaden as research continues to push the forefront of what cellular materials are capable of through the development of material science and fabrication technologies [9].

Other than medical implant and heat-exchanger devices, honeycomb structures have found increasing applications in almost every industry, and other advanced cellular materials, due mainly to the new material and fabrication technologies. Some detailed applications that increasingly make use of such honeycomb structures due to design flexibility and the chance to modify mechanical properties according to needs are listed below [10][11][12] and shown in Figure 1:

1. Aerospace and Aviation: Honeycomb structures are used for parts in aircraft and spacecraft, exhibiting a high strength-to-weight ratio, which is basically important in fuel efficiency [13].
2. Automotive Industry: The Honeycomb structure in the automotive industry is used in the energy absorption systems, like crumple zones, bumpers, and body panels to enhance the safety and efficiency of mechanisms [14].
3. Architecture and Construction: Honeycomb panels find their applications in modular construction and prefabricated building systems, showing very good stiffness and thermal insulation with minimal material consumption [15].
4. Sporting Goods and Protective Gear: The shock absorption and lightweight nature of Honeycomb structures make them ideal for helmets, protective padding, and high-performance sports equipment [16].
5. Energy Storage and Renewable Energy: Honeycomb structures are used in batteries, wind turbine blades, and solar panels, optimizing performance and reducing weight [17].

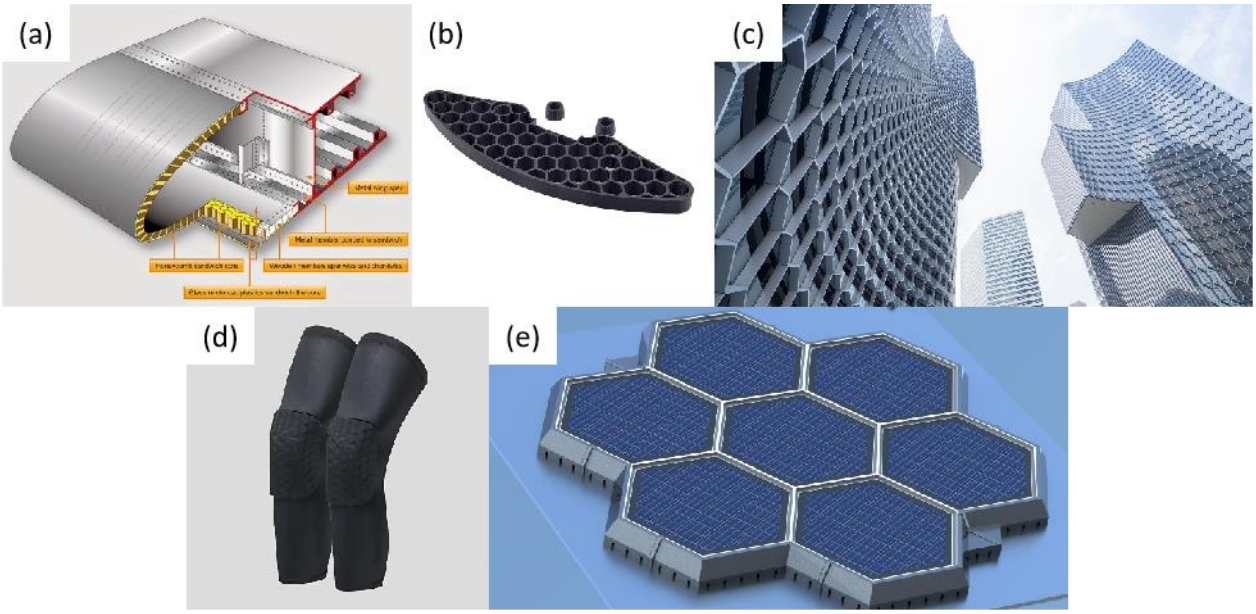

Figure 1 (a) Aluminum honeycomb panel on airplane [18]; (b) Honeycomb Front Bumper [19]; (c) Honeycomb-patterned facades building [20]; (e) Honeycomb Impact Protection [21]; (f) Honeycomb-like solar tile [22].

1.4 Traditional Manufacturing Methods for Cellular Materials

Extrusion and corrugation are widely adopted by industry as the major conventional techniques for the manufacturing of cellular materials with the configuration of honeycombs but pose serious drawbacks. First, there is very small freedom of design for current methods since most of them depend upon a predefined geometry. Limiting geometries therefore create minimal capacity to build or construct complicated or special designs. This inflexibility in design has somewhat impaired the potential for application-based optimization of honeycombs where specific mechanical property tuning may be necessary.

Secondly, conventional methods of fabrication are most apt for rigid materials, like metals or some kinds of polymers, which would not suffer from the extrusion or corrugation process [23]. This is less tolerant for fragile material or sensitive material in a low temperature; hence, it limits the kind of material that may be employed [24].

Besides, various traditional techniques present a set of processing challenges. Such multi-step processes generally are dependent on special equipment or tools/dies, which corresponds to longer times, higher costs, or lower scalability [25]. Another disadvantage is the lack of precise control over mechanical properties, since conventional methods can propose

only limited capability to appropriately tune mechanical properties like stiffness, strength, and energy absorption. This lack of control restricts the ability to optimize or customize honeycomb structures for particular performance requirements [26].

Finally, conventional methods are typically typified by the generation of much waste. In such a process as extrusion, scraps may be produced that have to be either recycled or disposed of, with extra steps involved in processing to handle the waste and loss of material [27].

1.5 Transition to Additive Manufacturing (AM)

With the development of manufacturing technologies, Additive Manufacturing has become the game-changing process that enables the elimination of most deficiencies stemming from traditional processes [28]. Also traditionally known as 3D printing, AM bestows unparalleled design freedom while enabling the fabrication of truly complex geometries that had remained unattainable yet. This technology enables one to precisely control cellular materials, including cell size, variation in wall thickness, or unit cell topology. This level of personalization is allowed by the AM, which opens a whole new dimension in optimizing mechanical properties like stiffness, strength, and energy absorption for specific applications [29].

Compared to the traditional methods, AM has several advantages, including less material waste and reduced lead times, which can make it a perfect solution for manufacturing complex honeycomb structures [30]. The most salient advantages of AM in manufacturing multi-material and hierarchical designs can further expand the performance envelope of cellular materials [31].

Specifically, the versatility of AM enables honeycomb structural design parameters—such as wall thickness and cell topology—to be modified with no problem. It has great consequences in the tailoring of honeycomb structures' mechanical properties and allows engineers to meet specific performances in either energy absorption enhancement or optimization of the strength-to-weight ratio [32]. These enable the effective fabrication of complicated multiscale structures made possible by AM and opened up new ways toward developing smart hierarchical Honeycomb structures.

1.6 Advanced Honeycomb Design: Cell Topology, Wall Thickness, and Hierarchical Structures

With the wide applications of honeycomb structures, many studies have been conducted to make their properties suitable for specific applications. Among them, cell topology and wall thickness are identified as the two most important design parameters. Several mechanical properties, such as stiffness, strength, and energy absorption, have been improved by optimizing the geometric arrangement of cells and changing the thickness of the walls. However, most of these design parameters, even though offering significant improvements, are usually confined to one scale beyond which further performance enhancement is not possible.

Given this, more complicated, multiscale designs are focused on by researchers nowadays in order to surmount the limitations. Introducing various hierarchical levels within honeycomb structures enables one to additionally improve the mechanical properties. As expected, these multi-scale or hierarchical Honeycomb structures can indeed exhibit better properties, for instance, higher energy absorption and more uniform distribution of stress compared to their more conventionally single-scale counterparts. Generally speaking, hierarchical design methods may be divided into two categories: reinforcing cell walls or joints/nodes enhancement.

1.7 Hierarchical Honeycomb Design, Manufacturing Challenges, and New Implementation Method

While hierarchical honeycomb structures have greatly improved mechanical property and energy absorption associated with their use, even the advancement of AM technologies does not easily fabricate them. Truly multiscale design fabrication requires high-resolution AM equipment, in particular at smaller length scales, which usually involves a sacrifice in production speed and volume. This often limits large-scale use of hierarchical honeycombs. The manufacturing constraints deal with speed and cost efficiency when dealing with complex multi-scale geometries requiring accurate control in printing parameters and material placing.

To address these challenges, a novel design and implementation method for hierarchical honeycomb structures has been

proposed in Figure 2. It applies Fused Filament Fabrication (FFF), a common AM technique, to fabricate hierarchical Honeycomb structures that integrate foaming and solid components. This enables a sophisticated material distribution by using, on the one hand, regular PLA for structural integrity combined with a foaming approach in regions that need lighter material for sandwich structures—a great technique to produce engineered porosity and mechanical characteristics.

By optimizing printing patterns and specific printing parameters, such as nozzle temperature, printing speed, and material flow, hierarchical honeycomb structures could be fabricated with good effectiveness, achieving controlled porosity—a critical factor in mechanical performance, particularly for energy absorption. In addition, the ability to further refine both the printing process and the design elements extends the traditional design space of honeycomb structures into unexplored regions, enabling unprecedented performance in applications that require high energy absorption combined with structural efficiency.

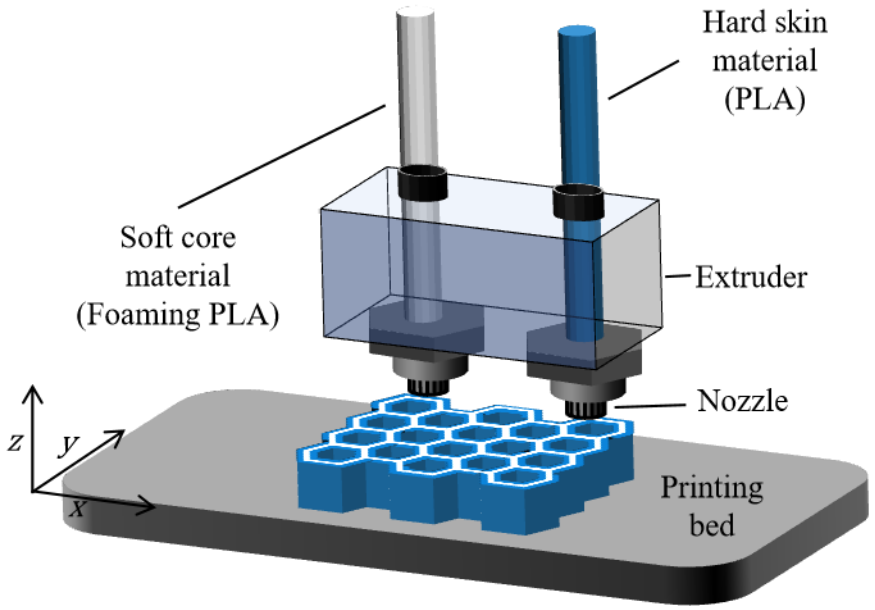

Figure 2 3D schematic of multi-material FFF printing of hierarchical honeycomb structures in this study.

Through this method, the limitations of traditional manufacturing are mitigated, and the performance of honeycomb structures is enhanced, particularly in terms of weight reduction and energy absorption. The integration of solid and foaming materials within a single structure enables the optimization of both strength and flexibility, further enhancing the functionality of hierarchical honeycombs for various engineering applications.

To achieve this goal and further refine the design and manufacturing approach for hierarchical honeycomb structures, we conducted a thorough literature review. In Chapter 2, we will discuss the key advancements in manufacturing methods, cellular material design, and hierarchical structures, providing a foundation for the proposed innovations in this work.

Chapter 2: Literature Review

2.1 Overview of Manufacturing methods

2.1.1 Conventional Manufacturing

Traditionally, cellular materials are produced by well-established techniques such as extrusion, corrugation, and lamination [33][34][35]. These methods have certainly found widespread application but come with certain limitations in the design freedom, scalability, and compatibility with materials [36]. Some conventional manufacturing processes are summarized below and shown in Figure 3.

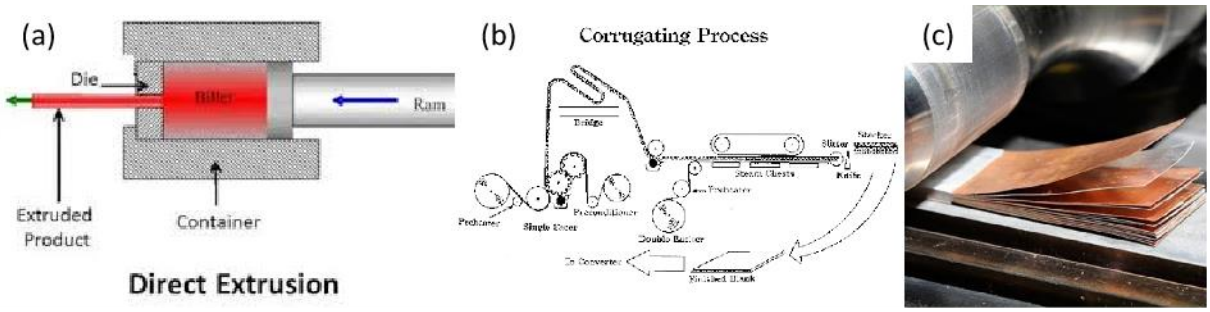

Figure 3 (a) Direct extrusion[37]; (b) Corrugation process [38]; (c) Lamination of metal [39].

2.1.1.1 Extrusion

Conventionally, one of the most common fabrication techniques of cellular materials, particularly polymeric foams, is extrusion. The method consists of forcing the material through a die to create continuous profiles with precisely defined cross-sectional shapes [40]. During the process of cellular material manufacturing, gas or a blowing agent is mixed into the molten polymer to form a porous, foam-like structure. This explains the widespread popularity of extrusion—it enables manufacturing in large quantities at relatively low cost [41]. However, certain major barriers remain with extrusion. While it works well for creating simple, uniform shapes, it struggles to fabricate complex cellular materials or tailored designs. Furthermore, managing porosity and cell size can be problematic, which limits the ability to modulate mechanical properties for specific applications [42][43]. Most cellular materials produced through extrusion exhibit isotropic properties. This uniformity can be a drawback in applications that specifically demand anisotropic

mechanical performance [44].

2.1.1.2 Corrugation

Among various techniques, corrugation is the most common method for producing honeycomb structures in packaging and construction. The procedure involves shaping flat sheets into an undulating pattern of alternating ridges and troughs, which are then joined together to create the honeycomb structure [45]. Corrugated honeycombs offer high strength and stiffness with minimal material usage, making them well-suited for lightweight designs [46]. Although corrugation is simple and cost-efficient, it is constrained by the geometry of the corrugated sheets. This method generally creates two-dimensional structures with fixed cell shapes, most commonly hexagonal. Such limitations reduce design flexibility and make it challenging to customize features like cell sizes, wall thickness, or more complex geometries for advanced engineering needs [47]. Furthermore, corrugated honeycombs often rely on adhesive bonding, which can introduce weak points into the structure, potentially reducing its overall mechanical performance.

2.1.1.3 Lamination

Lamination is another traditional method for producing cellular materials, particularly honeycombs [34]. In this process, layers of flat material (often paper, aluminum, or polymers) are stacked and bonded together, with each layer containing a cut pattern that, when expanded, forms a cellular material. This technique is extensively used in the aerospace industry due to its ability to produce lightweight, high-strength structures with exceptional load-bearing capacity. However, lamination, much like corrugation, comes with certain drawbacks. The precise alignment and bonding of layers required in this process can lead to manufacturing complexities and extend production times. Furthermore, laminated structures typically exhibit uniform cell sizes and shapes, which limit their adaptability for applications requiring non-uniform or graded structures [48]. Additionally, the use of adhesives in lamination often undermines the thermal and environmental stability of the structure, as adhesive bonds tend to weaken under extreme or harsh conditions.

2.1.1.4 Foam Casting and Molding

The most common techniques for producing polymeric foams and other cellular materials include foam casting and injection molding. In these processes, a liquid polymer or polymer mixture is introduced into a mold, where it is allowed to expand and solidify, creating a porous structure. These methods are advantageous in their ability to produce complex

three-dimensional shapes and integrate cellular materials with other components during the molding process [49]. The major challenge with foam casting and molding lies in controlling the porosity and cell size distribution throughout the material. Achieving uniformity in the cellular material is often difficult, particularly when working with large or complex molds. Additionally, these methods are largely limited to specific material types, such as certain polymers, and are unsuitable for more delicate or high-performance materials that require precise control over the microstructure [50].

2.1.1.5 Challenges in Traditional Manufacturing

Traditional manufacturing techniques of cellular materials have effectively served industries over decades, ranging from cost-effective to scaled-up applications. However, at a point when demands for value-added and functional materials were raised, the shortage of conventional methods appeared clear [51]. The main challenges involve [52]:

1. Design Flexibility: Most of the conventional methods, such as extrusion and corrugation, are bound to simple geometries and uniform structures. This narrows the possibility for creating complex or customized designs for more specialized applications.
2. Material Compatibility: Most traditional methods are more adapted to rigid materials, such as metals or some polymers, while a number of modern, more delicate, or high-performance materials can require very specific processing conditions.
3. Control of Mechanical Properties: Most of the traditional methods hardly achieve mechanical property control, such as control of stiffness, strength, and energy absorption, because of the difficulties in porosity, cell size, and material distribution control.
4. Scalability and Production Costs: While the conventional methods are much effective for bulk production, they may introduce higher costs of production and longer processing times in the development of more complex or multi-functional cellular materials.

In response to the limitations of traditional manufacturing techniques, the evolution of additive manufacturing techniques has opened new possibilities in the fabrication of cellular materials at small size levels. AM allows for greater design flexibility and the creation of complex geometries and graded structures impossible to achieve with

traditional methods [53][54]. Moreover, AM permits multiple material integrations and tight control over microstructures to achieve the next generation of high-performance cellular materials [55][56][57].

2.1.2 Additive Manufacturing (AM)

Additive Manufacturing, well known as 3D printing, is one of the most disrupting technologies in these times, with huge interest at industrial and research levels. The development of new materials, the improvement of printing techniques such as SLM, FDM, and SLA, among others, innovations in multi-material and multi-functional printing, and the post-processing methods are part of AM [28]. The various fields in which AM finds applications include significant use in the aerospace, automotive, health, architecture, consumer goods, and electronics industries. In comparison with conventional approaches to manufacturing, AM is superior on many aspects: free from typical issues, such as design freedom, reduced prototyping, personalization of parts, reduction in wasted material, reduction of intermediate steps in the supply chain, and overall reduced product cost [29][30]. The reason may be that AM can perfectly fit into the honeycomb manufacturing technique due to its overcoming of the critical defects of the conventional techniques of fabrication:

1. Design Freedom: Additive manufacturing can offer unmatched design freedom in developing complicated honeycomb geometries [31]. With 3D printing, designers will be able to create complex cell structures by changing cell dimensions and wall thicknesses, even evoking graded or customized properties within the honeycomb structure. This would permit the possibility to optimize for specific application requirements based on maximization of the strength-to-weight ratio or enhancement of energy absorption [32].

2. Material Versatility: Additive manufacturing enables a wide range of materials, including polymers, metals, ceramics, composites, and even bioactive materials [58]. This versatility enables the fabrication of honeycomb structures using materials with tailored mechanical properties, thermal characteristics, or specific functional requirements. Besides this, multi-material 3D printing technology enables a combination of different materials within honeycomb structures, thus further expanding their application range [59].

3. Precise Control and Customization of cell geometries: Additive manufacturing allows the production process to be finely controlled, such that very careful control can be given to cell geometry, dimensions, and wall thickness [60].

The layer-by-layer deposition or solidification process, tunable at a micro scale, results in a very accurate and consistent honeycomb structure. This can be a great way of optimizing the mechanical properties for given performance criteria [61][62][63].

4. Lessened Generation of Waste: The process is additive, meaning that it builds up the desired structure with only material deposition [64]. Traditional subtractive manufacturing techniques involve removing material from blank, which often leads to waste. Additive manufacturing techniques result in much less waste generated from materials, maximize the material efficiency, and, ultimately, have reduced environmental impacts [65].

5. Rapid Prototyping and Shorter Lead Times: Additive manufacturing allows for rapid prototyping and iterative design cycles that greatly reduce the development and refinement time of honeycomb structures. Modifications in design can be easily made, thus quicker design iterations and shorter lead times. This agility is especially helpful for industries where there is a need for rapid development and testing of either prototypes or customized products [66].

Additive manufacturing is particularly appropriate for honeycomb structure realization, a subset of additive manufacturing processes known as the Fused Filament Fabrication (FFF) process, thanks to many advantages. Inherent in additive manufacturing, FFF offers design flexibility that provides the potential for optimization of honeycomb structures with respect to specific applications and makes it feasible to achieve geometrically complicated structures, difficult to manufacture by conventional means [67]. In addition, FFF boasts relatively low manufacturing costs compared to other additive manufacturing processes. It therefore stands out in the application of prototyping, small-scale production, and other areas where cost constraints may be a major issue [68]. Besides, FFF is also characterized by high printing speed, enabling fast fabrication of honeycomb structures. This rapid-production capability is useful for those applications requiring rapid prototyping, iterated designs, or short lead times, and enables efficient investigation of various honeycomb geometries, material combinations, or changes in cell geometry. Besides that, FFF printers can control with high precision the temperature at which the melting of filament occurs, as well as the quality of the final product through changes in nozzle and build plate temperature [69].

2.2. Review of Cellular Materials

2.2.1 Classification of Cellular Materials

Cellular materials are materials that consist of an interconnected network of struts or plates, forming intricate three-dimensional architectures with significant porosity [70]. The properties can be tuned through changes in the meso- or microstructure. When struts are subject to predominantly axial tension or compression, a high stiffness-to-weight ratio develops, making stretch-dominated cellular materials ideal for lightweight applications where structural efficiency is essential. In contrast, bending-dominated structures are characterized by a plateau in their stress-strain curve, making them particularly effective for energy absorption [71]. Auxetic cellular materials have a negative Poisson's ratio, meaning they expand laterally when stretched, providing unique mechanical behaviors beneficial in a wide variety of engineering applications [72].

Furthermore, in addition to their mechanical performance, cellular materials are being engineered for electromagnetic wave absorption and efficient heat transfer, making them ideal candidates for multi-functional, lightweight parts [73]. Material systems with these features have been studied to develop specialized properties, including a high stiffness-to-weight ratio, negative Poisson's ratio, and high energy absorption capacity. These characteristics are achieved through precise tailoring of meso- or microscale architectures in cellular materials [74].

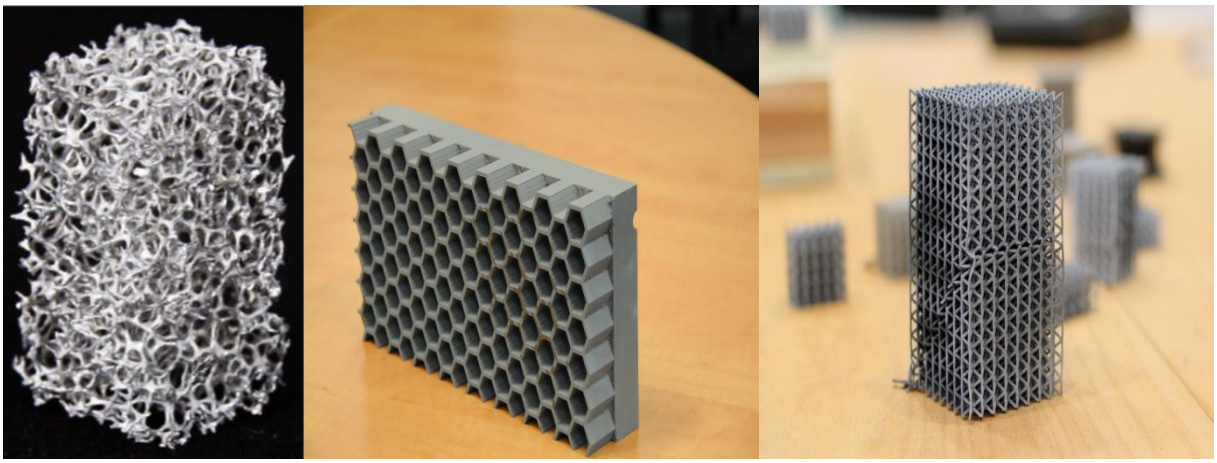

Figure 4 Aluminum Foam[75], Honeycomb Structure, ©ESA [76] and Lattice Structure[77]

This material, recognized for its porous structure and impressive strength-to-weight ratio, has drawn significant interest in disciplines like engineering, materials science, and biomimetics. Classification is essential to organizing and

understanding the extensive variety of cellular materials, which can be divided based on their structural traits at two-dimensional (2D) and three-dimensional (3D) levels.

In the two-dimensional (2D) realm, cellular materials are classified by the shape and arrangement of their unit cells [78]. These arrangements are further divided into regular and irregular arrangements [79]. Regular arrangements include honeycomb and lattice structures, where cells are uniformly organized. In contrast, irregular arrangements mainly consist of predominantly foam structures, characterized by a random distribution of cells [80].

On a three-dimensional (3D) level, cellular materials are broadly classified into three categories based on their microstructure: foams, honeycombs, and lattice structures [81][82][83][84].

Foams comprise randomly arranged interconnected cells or voids [85]. These cells vary in shape and size, creating a highly porous structure typically produced by introducing bubbles into a liquid precursor that solidifies into foam [86]. Foams are Notable for being lightweight, highly porous, and excellent in energy absorption, thermal insulation, and acoustic dampening [87].

Honeycomb structures feature a regular hexagonal arrangement akin to a beehive. The cells are usually elongated with walls perpendicular to adjacent cells [88]. The manufacturing of honeycomb structures involves traditional methods like extrusion or modern techniques such as additive manufacturing [89][90]. Honeycombs offer a high stiffness and strength-to-weight ratio, making them ideal for load-bearing and impact-resistant applications [91].

Lattice structures encompass a variety of periodic or non-periodic architectures, including truss-based configurations, and can be composed of sheets, struts, volume or shell-like elements. Their geometry and orientation can be tailored to achieve specific mechanical properties [92]. The unit cells can be either regular or irregular, with struts of varying orientations and cross-sectional shapes. Lattice structures can be precisely controlled in terms of geometry and properties and are typically fabricated using advanced technologies like 3D printing, CNC machining, or casting [18]. These structures are Renowned for high strength, stiffness, and customizable mechanical properties by modifying strut geometry and arrangement and often used in applications requiring structural components with minimal weight and high strength [93].

Each type of cellular material exhibits distinct characteristics, making them suitable for specific applications based on

their mechanical performance, fabrication potential, and structural demands [94].

2.2.2 Strut and sheet-based structures

In structurally regular cellular materials, lattice structures can be further classified into strut-based and sheet-based structures based on the primary structural elements present in the lattice [95][96][97].

1. Strut-Based Structures: In strut-based lattice structures (Figure 5), the primary load-bearing elements are the pillars or beams that connect the lattice units. These struts support the applied loads and maintain structural integrity. A notable example of a strut-based structure is the truss structure. Truss structures are composed of interconnected struts arranged in networks of triangles or other polygons. These struts act as load-bearing elements, efficiently transferring forces between designated points. Renowned for their ability to achieve high strength and stiffness with minimal material usage, truss structures excel in optimizing both material efficiency and mechanical performance [98].

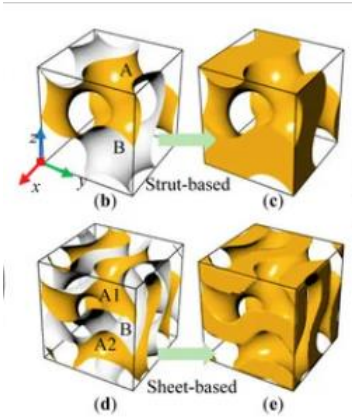

Figure 5 Sheet and Strut-based Gyroid Structure [99]

2. Sheet-Based Structures: A sheet-based lattice structure is a type of periodic cellular material characterized by thin, interconnected sheet-like elements instead of discrete struts or beams. These structures are often inspired by natural forms, such as trabecular bone or biological shells, and can provide superior mechanical properties compared to truss-based lattices. A prominent example of a sheet-based structure is the Gyroid lattice, which is defined by a repeating Triply Periodic Minimal Surface (TPMS). The Gyroid lattice features an intricate network of interconnected curved sheets or struts, offering a unique combination of strength and flexibility. This complex

arrangement enables Gyroid lattices to achieve excellent mechanical performance, making them suitable for applications requiring a balance of rigidity and adaptability [100].

Triply Periodic Minimal Surface (TPMS) are mathematically defined surfaces in three-dimensional (3D) space, distinguished by their 3D periodicity, zero mean curvature, and expansive surface area [101]. TPMS exhibits periodic minimal structures across all three dimensions, forming a seamless, continuous pattern without boundaries or edges. These surfaces can extend infinitely in all directions while maintaining their overall structural integrity. This characteristic grants TPMS unique mechanical properties, such as excellent load distribution and lightweight structural efficiency, making them highly desirable in advanced material applications [102].

Additionally, within regular materials, there exists another type of cellular material known as honeycomb structures (as shown in Figure 6), which can be classified into several common types:

1. Regular Honeycomb: This structure is defined by uniformly arranged hexagonal cells. The main walls between the cells are essentially straight and parallel, presenting an efficient design for uses requiring high strength-to-weight ratios [103].

2. Asymmetrical Honeycomb: Composed of hexagonal cells in which the offset of the cells is asymmetrical—the cells are not perfectly aligned—such that an alternating pattern is achieved in the structure. The asymmetrical honeycomb yields better shear performance and normally finds application in areas needing high shear [104].

3. Flex-Core Honeycomb: In this cell structure, the cell size through the structure is variable, tapering from large to small and vice versa. The flex-core design gives better energy absorption since it has a higher power of energy dissipation over other geometrical configurations upon impact, thus making it suitable where high energy dissipation levels are required [105].

4. Overexpanded Honeycomb: An overexpanded honeycomb structure is generated by stretching a regular honeycomb in one or more directions. Compared to the original design, cell sizes in the overexpanded honeycomb structure are larger. It can provide more flexibility, and it allows for greater deformation under tensile load while preserving the integrity of the structure [106].

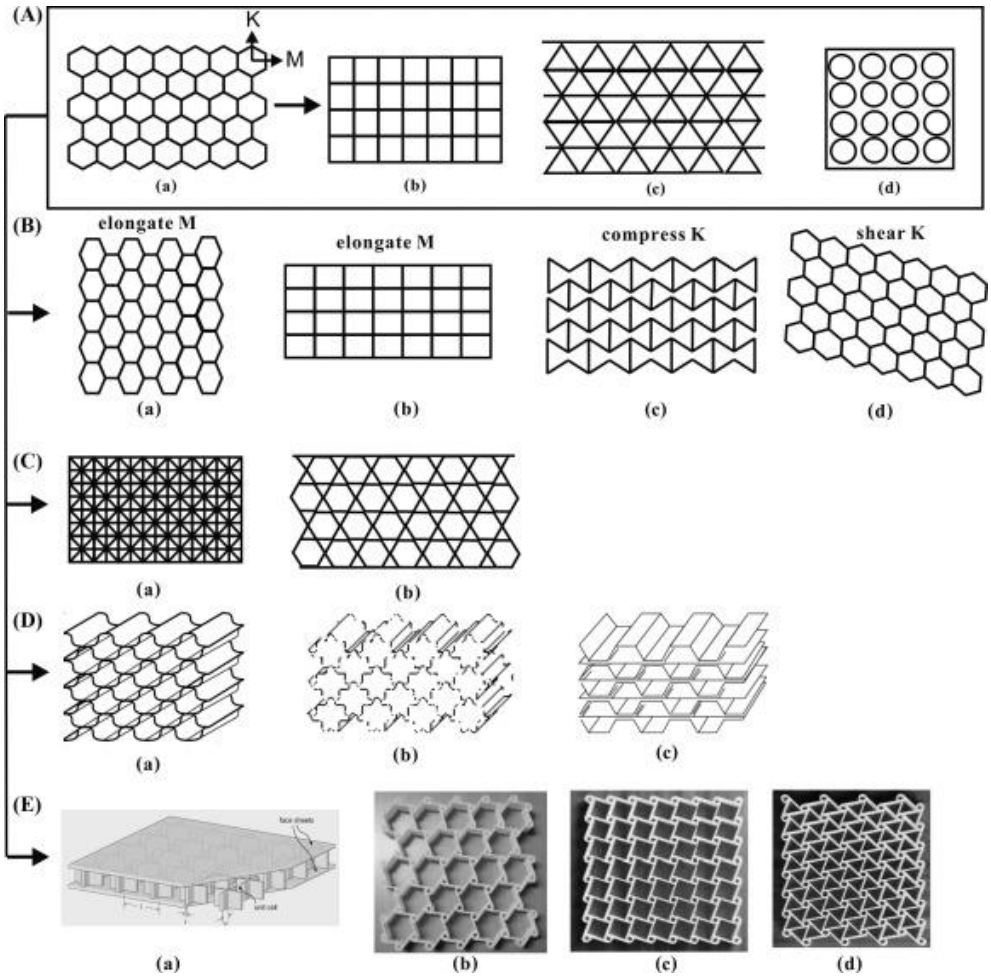

Figure 6 Periodic honeycombs with various cell shapes. (A-a) Regular hexagonal cell; (A-b) square cell; (A-c) triangular cell; (A-d) columnar cell; (B-a) OX cell; (B-b) rectangular cell; (B-c) reentrant hexangular cell; (B-d) asymmetrical honeycomb; (C-a) square supercell constructed from mix of squares and triangles; (C-b) Kagome cell; (D-a) flex-core cell; (D-b) double-flex cell; (D-c) reinforced hexagonal cell; (E-a) truncated-square cell; (E-b) tri chiral cell; (E-c) tetrachiral cell and (E-d) hexachiral cell. K and M denote two arbitrary vector axes in space cell [107].

2.2.3 Cellular Materials Fabrication

In the case of advanced cellular materials created, for example, by various AM techniques such as Selective Laser Melting (SLM), Fused Filament Fabrication (FFF), and Stereolithography (SLA) (Figure 7), these methods enable the layer-by-layer creation of cellular materials. This provides an excellent avenue for having complete control of the pattern and material composition to realize complicated cellular materials [108].

Conventionally, various techniques are employed for the fabrication of materials of irregular structure, including

foams—cellular materials consisting of gas-filled voids or cells enveloped in solid material:

1. Foam Casting: Liquid precursor or a mixture is poured into the mold or template. The process therefore follows solidification and cellular development with the help of the appropriate chemical reaction or curing of the precursor [109].

2. Foam Extrusion: A method involves forcing a mixture of solid material and gas through a die. In exiting the die, gas that is expanding within the material forms a cellular foam [110].

3. Foam Injection Molding: This technique involves the injection of the molten material with the blowing agent into a mold. While cooling down, with the solidification of the material, the blowing agent expands to create cells inside the material and a cellular material [111].

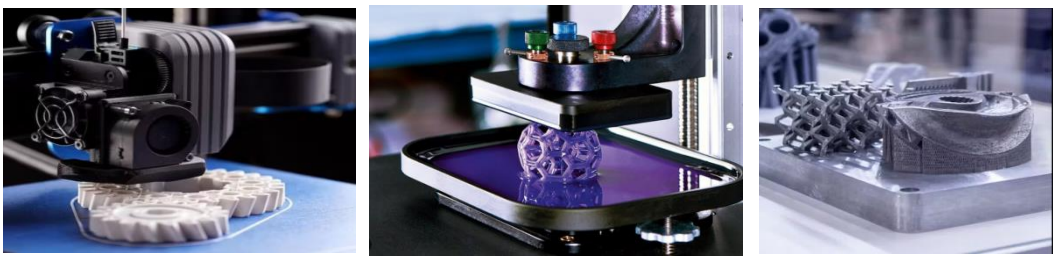

Figure 7 FFF, SLA and SLM AM Printing Method [112][113][114]

2.3 Design Parameters and Deformation Mode of Cellular Materials

Most of the research has focused on the design of cellular materials, particularly honeycomb structures. The characteristics of honeycomb-structured materials have recently undergone extensive study to achieve specific properties. Cell topology and wall thickness have emerged as the two most critical design parameters. Distinct topological configurations exhibit different mechanical behaviors, prompting exploration into various structures, such as hexagonal, square, and re-entrant honeycombs to optimize mechanical behavior [115][116][117][118][119]. Additionally, studies have examined the impact of topological defects [120] and unit cell size [121] on the mechanical properties of these materials. Research has shown that topology optimization can enable specific functions, such as amplified passive deformation [122] or significantly enhanced electrical insulation performance [123]. Additionally, auxetic structures like re-entrant auxetic honeycombs and S-shaped chiral structures have demonstrated superior

mechanical properties [124].

While most current designs of honeycomb structures emphasize cell topology and the influence of geometric form on overall performance, a wall thickness-oriented design approach has recently emerged. Research has explored the effects of wall thickness on structural design [125], mechanical properties [126][127][128][129], deformation modes, stress distribution, and compressive behavior [130]. Additionally, the non-linear relationship between non-uniform wall thickness and mechanical properties has been revealed [131][132]. Innovative design strategies, such as the novel re-entrant honeycomb structure [133] and the embedded enhanced honeycomb structure [127], highlight the potential of graded wall thickness in enhancing material properties.

Instead of focusing solely on unit cell topology and wall thickness at a single design scale, some recent research has demonstrated that multi-scale or hierarchical honeycomb structures can achieve superior properties. Hierarchical honeycomb structure designs are mainly categorized into two strategies: reinforcing the walls or reinforcing the joints/nodes.

1. Wall Reinforcement: This approach includes designs such as a bionic hierarchical structure on the cell walls [134], adding local hexagonal structures as resonance systems on the walls [135][136], and substituting the cell walls with negative Poisson's ratio auxetic honeycombs and chiral honeycombs [137][138]. These modifications often enhance the energy absorption efficiency and stiffness of the structure.

2. Node or Joint Reinforcement: To reinforce the nodes or joints, researchers have explored various methods, including nesting and assembling node-locked components of specific shapes [139], adding self-similar inclusions at the nodes [140], and adding three different structural variations at the joints [141]. Additionally, some studies have designed energy-efficient absorbing structures from a biomimetic perspective [142]. And the coupling effects between the self-similar hierarchical characteristics of honeycomb structures and their dynamic mechanical properties have also been investigated [143]. Compared to the original design, these hierarchical designs can significantly improve energy absorption capacity, plateau stress, and impact load efficiency.

Multiscale design is a systematic process involving multiple steps. First, the overall structure is determined, and the

desired length scales or levels of hierarchy are identified. Then, appropriate materials are selected for each length scale. At the largest length scale, the macrostructure is designed by determining the shape, size and arrangement of the cells. Based on macro cells, the mesoscale structure is designed to incorporate smaller cells or lattice-like structures. At the microscale, smaller features such as microcells or porous walls are introduced into the meso cells. The interconnectivity between cells at all scales is optimized and the possibility of introducing material gradients in the cellular material is considered. The design is then simulated and optimized using computational tools or simulation methods. The feasibility and limitations of the selected manufacturing method are evaluated, and finally the prepared multiscale cellular materials are tested and characterized [144][145][146][147].

In addition to single-scale design optimization, hierarchical honeycomb structures have attracted much attention due to their ability to provide superior mechanical properties. This hierarchical structure enables it to exhibit multiple properties and functions. By adjusting the organizational form and characteristics of each layer, honeycomb structures can be engineered to achieve desired mechanical properties, such as improved strength, hardness, or energy absorption [148]. The common levels of hierarchical structure in cellular materials include:

1. Macrostructure: At the highest level, the cellular material behaves as a homogeneous material. The macrostructure can take various forms, such as foams, honeycombs, lattice structures, or other specific geometries tailored for the applications [149]. The choice of macrostructure significantly influences the overall mechanical performance and suitability in different applications.

2. Cellular-Level Structure: At the next level of hierarchical design is the basic cell structure, which is the basic building block of cellular materials. The shape, size, and connection of the cells can be flexible and their performance can be optimized by adjusting the geometric design parameters [150]. By modifying these parameters, specific mechanical behaviors can be optimized, such as load distribution and energy dissipation capacity.

3. Strut or Wall Layer Structure: Within each unit cell, there are internal struts or walls that connect the faces or vertices of the unit. These struts or walls provide structural integrity and load-bearing capacity. The arrangement, shape, and size of these struts significantly affect the mechanical properties of the material.

Depending on the structural parameters, the material can exhibit either bending-dominated or stretching-dominated behavior, each offering different mechanical characteristics [151].

4. Subcellular or Microstructural Level: Within the struts or walls, there may be more detailed microstructural features or variations. This level includes details such as tiny pores, surface roughness, or material gradients, which affect the material's strength, stiffness, and energy absorption properties [152]. These microstructural details are crucial for fine-tuning the properties of cellular materials, especially in applications that require specific mechanical properties.

The multiscale design of hierarchical honeycombs introduces new deformation modes, unlike the deformation modes of more conventional honeycomb structures. For instance, the deformation mode in traditional honeycombs is often bending-dominant—that is, cell walls bend under load—or stretching-dominant, in which the walls are subjected mainly to tension or compression [153]. The main difference between such bending and stretching dominated structures lies in the type of mechanisms occurring within:

1. Bending-dominated structure: In general, the struts or walls belonging to cellular materials are dominated by bending stresses. Subsequently, the struts buckle or bend by dissipating the applied compressive, bending, and other external loads. Such bending-dominating structures have struts and/or walls long enough while slender, exhibiting high amenability to deformation or flexibility, for instance. These structures are outstanding for their excellent energy absorption properties and resistance to impacts of greater magnitudes [154].

2. Stretching-dominated structure: A stretching-dominated structure refers principally to the resistance against most tensile or stretching stresses over the struts or rather walls. When subjected to external loadings, the struts effectively disperse the strains by lengthening or stretching under such applied forces. This structure generally consists of shorter and sturdier struts or walls, yielding high stiffness and strength. These structures have the ability to bear loads effectively and show superior mechanical performance under tensile stresses [155] (Figure 8).

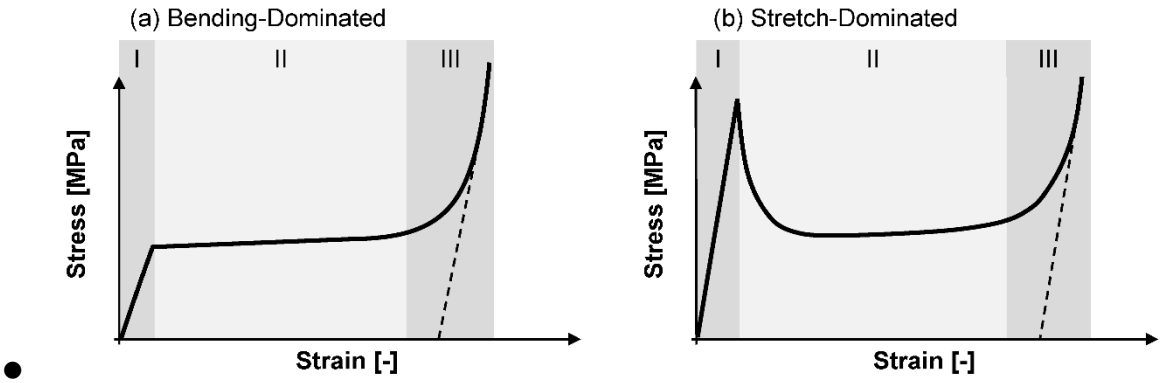

Figure 8 Bending and Stretch-Dominated Stress-Strain Curve [156]

Which of the two modes of deformation, bending or stretching, dominates in cellular materials depends on the geometric proportions and connectivity of the struts or walls [157]. It is the relative length and thickness and the way in which the structural elements are assembled that dictates the primary load-carrying mode. Thus, for example, when the length-to-thickness ratio of the struts increases, bending becomes increasingly favored, whereas a reduction in this ratio favors the predominance of stretching. Optimal honeycomb-like materials in any particular application, for instance, energy absorption, structural support, or even load-carrying capacity, are achieved by these parameters. Note that honeycomb-like material would be able to exhibit either or both of the bending and stretching behaviors under different load conditions and properties. The balance between bending and stretching controls the whole mechanical response and performance in such materials [158].

In summary, recent studies on mechanical properties in honeycomb structures manufactured by FFF show promising results, though studies on process parameters and hierarchical cell designs remain few. Hence, the current work will present a methodology to improve the mechanical performance of honeycomb structures for energy absorption using FFF technology with foamed PLA. It consists of two major parts: first, optimization issues concerning mechanical properties of the FFF process parameters; second, it researches the influence of different hierarchical cell design variants on energy absorption and load distribution in such structures. The results obtained within this work will contribute to a deeper understanding of how to design and manufacture high-performance, energy-absorbing cellular materials. Chapter 3 presents how the foaming PLA filaments were fabricated, including selecting the material, calibrating the flow multiplier, and optimizing printing parameters—nozzle temperature and extrusion multiplier.

Chapter 3: Fabrication of Foaming PLA and Properties

This chapter provides detailed information on materials and its manufacturing process for designed hierarchical honeycomb structures. Particularly, Section 3.1 introduces the general fabrication process of parts made of PLA and foaming PLA materials. The process parameters used in this fabrication process will be discussed in Section 3.2. Among these process parameters, the flow multiplier for foaming materials needs to be tuned for different nozzle temperature, a detailed procedure on tuning of flow ratio of foaming materials is presented in Section 3.3. The impacts of the fabrication parameters on the porosity and mechanical properties will be discussed respectively in Section 3.4 and Section 3.5

3.1 Materials & Fabrication Process

To fabricate materials with pore on micrometer scale, Esun PLA-LW lightweight PLA 3D printing filament is used as foaming materials. This filament is manufactured using a thermoplastic polymer matrix, in which a physical or chemical blowing agent is integrated. The manufacturing process of filaments involves a precisely controlled extrusion where temperature, pressure, and shear forces are meticulously adjusted to ensure the uniform distribution and retention of the blowing agent in the polymer matrix, a crucial step that determines the filament's foaming potential [159].

As this foaming filament passes through the nozzle in high temperature range, typically from $210°C$ to $250°C$, the material expands and forms a foamed cellular material. By adjusting printing parameters such as flow multiplier and printing speed, uniform extrusion and stability of the foaming process can be ensured. After extrusion, the material cools rapidly and solidifies, retaining its expanded porous structure. Due to the increase in volume during the foaming process, the actual printed material volume is often greater than the volume of input filament. Therefore, calibration of the flow multiplier is necessary before printing to ensure precision bead width and structural consistency.

Specifically, in this research, the Bambu X1C printer *(Bambu X1 Carbon, Bambu Lab, China*) was chosen for its ability to switch materials during printing with a single nozzle, allowing precise transitions between base PLA and foaming PLA without the complexity of a dual-extruder setup. This approach reduces calibration challenges and prevents issues like print head misalignment. The printer also provides high-speed, accurate printing, making it ideal for producing the

multi-scale hierarchical honeycomb structures in this study.

Table 1 Process parameters of foaming PLA and solid PLA.

Setting name	**PLA**	**Foaming PLA**
Nozzle diameter	$0.4\ mm$	$0.4\ mm$
Layer height	$0.2\ mm$	$0.2\ mm$
Extrusion width setting	$0.4\ mm$	$0.4\ mm$
Print speed	$60\ mm/s$	$25\ mm/s$
Cooling setting	$No\ cooling$	$No\ cooling$
Bed temperature	60℃	60℃
Retraction	YES	NO
Nozzle temperature	190℃	210℃ − 250℃
Flow multiplier	0.93	See in Section3.3

3.2 Fabrication Process Parameters

Like conventional solid PLA materials, process parameters in FFF process also play key roles on its microstructures and mechanical properties of fabricated foaming materials. The key process parameters are selected and summarized in Table 1. In Table 1, the process parameters for PLA is decided based on the previously published reference and suggested parameters from machine vendors.

As to foaming PLA, the same layer height and extrusion width as solid PLA is selected due to both of them will be used for the sample part printing. As to printing speed, due to the foaming process, which may affect thus the smaller printing speed is selected based on initial trial printing. As to nozzle temperature, it can control the foaming ratio. Thus, we select a temperature range rather than a certain values. The following contents of this section will discuss how this nozzle temperature will affect flow multiplier as well as the density and mechanical properties of fabricated PLA materials.

The first parameter is nozzle temperature, which usually ranges from 190℃ to 250℃. This parameter is crucial for influencing the polymers flow as well as in-situ foaming process. Specifically, in this study, three levels of nozzle temperature: 210℃, 230℃ and 250℃ are selected to achieve the different pore size and porosity of foaming materials. Experiments will be done to understand how the nozzle temperature will affect porosity, density and mechanical properties. Details will be discussed in Section 3.4 and Section 3.5. Additionally, the printing speed,

which varies from $10\ mm/s$ to $100\ mm/s$, also affects the foam's expansion and cell structure during extrusion [160]. In this research, printing speed of $25\ mm/s$ has been due to the optimal surface quality. In addition to that, this speed also prevents the foaming PLA from excessive expansion at high nozzle temperatures (250℃), which could otherwise result in nozzle blockage usually happened on high printing speed. At the same time, excessive expansion can also affect the extrusion width. Extrusion width (as shown in the Figure 9), this refers to the width of the material strand extruded through the nozzle. The extrusion width is typically determined by the nozzle diameter and layer height, and is specifically influenced by the printing speed, material flow properties, and nozzle temperature. In this study, a nozzle with a diameter of $0.4\ mm$ was used, with a layer height set at $0.2\ mm$, and the printing speed, as discussed in this chapter, was set at $25\ mm/s$. Extrusion width is a critical parameter in FFF printing, as it directly influences the deviation between designed and actual fabrication dimensions, as well as the bonding quality between adjacent tracks.

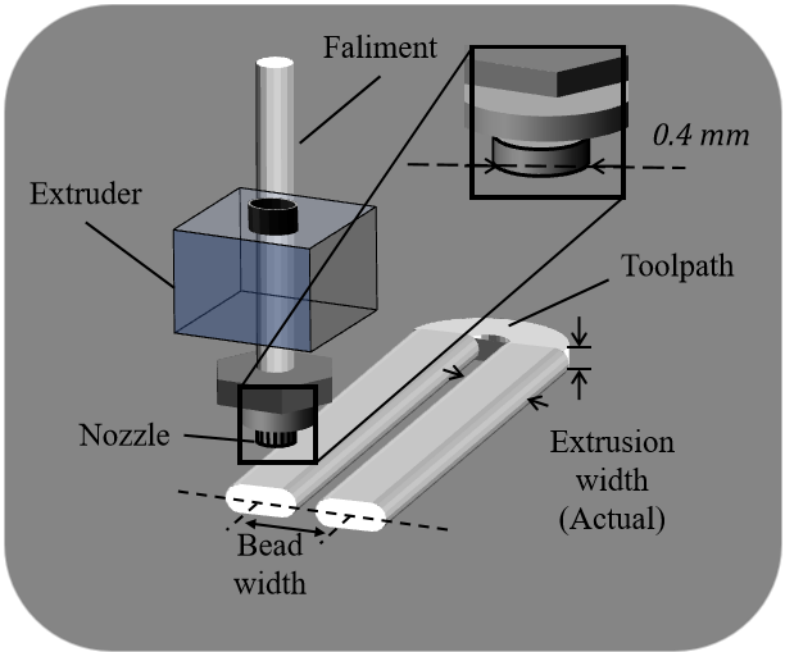

Figure 9 Toolpath and its relevant process parameters.

In the relationship between extrusion width and the actual fabrication dimensions, the material's flow-speed plays a critical role. Flow-speed not only affects the interlayer bonding strength but also determines the uniformity and stability of the material during deposition. In this research, flow-speed was controlled by the flow multiplier in the printing settings. In this work, the flow speed was controlled by the flow multiplier in printing settings. As one of the most important parameters in the control of material flow, precise adjustment of the flow multiplier allows compensation for

the changes in flowability due to changes in material viscosity or nozzle temperature; hence, the stability in the extrusion width. However, it is impossible to avoid the deviation in dimensions of real fabrication by relying only on theoretical settings; thus, other calibration steps will be needed. The next section gives a detailed explanation of the calibration steps for extrusion width by experimentally verifying the accurate extrusion width alignment with printing settings for better overall accuracy in fabrication.

3.3 Calibration of Extrusion Width

Given the different expansion rate of foaming PLA under different nozzle temperatures, the extrusion widths are calibrated at different nozzle temperatures by adjusting the flow multiplier. The flow multiplier controls the speed of extrusion volume, and by adjusting it, the expanded volume of the foaming material at different temperatures can be compensated for, ensuring the extrusion width matches the set constant value which should equal to extrusion width. A higher flow multiplier increases the amount of extruded material, resulting in a wider extrusion width, while a lower flow multiplier reduces the width. This calibration method ensures consistent printing accuracy and dimensional uniformity across different temperatures. Printing setting of foaming PLA is tabulated in below table. During the extrusion width calibration process, the variable substitution method was used for measurement. Specifically, Lidless-Single-Wall Cubes (LSC)were printed (as shown in Figure 10), and the actual extrusion width was calculated by measuring the actual thickness of the single wall (t_a).

In this study, fan cooling was intentionally omitted to avoid introducing additional variables and to maintain a controlled calibration process. Since the cooling effect varies with nozzle temperature, applying the same fan setting across different conditions could introduce inconsistencies in expansion behavior. Moreover, without forced convection, the material undergoes natural cooling, reflecting the intrinsic expansion characteristics of the foam PLA at different temperatures.

Table 2 Foam PLA initial printing parameters.

Setting name	Value
Nozzle diameter	$0.4\ mm$

Layer height	0.2 mm
Extrusion width (Designed)	0.4 mm
Print speed	25 mm/s
Cooling setting	No cooling
Bed temperature	60℃
Retraction	No
Nozzle temperature	210℃ 230℃ 250℃
Initial flow multiplier	90%

After applying the initial printing parameters detailed in the Table 2, initial t_a is measured. According to flow math in FFF process:

$$A_e = (e - h) * h + d * \left(\frac{h}{2}\right)^2 \quad (1)$$

$$A'_e = (e' - h) * h + d * \left(\frac{h}{2}\right)^2 \quad (2)$$

Where A_e is the actual cross-section area of extrusion width, A'_e is the designed cross-section area of extrusion width, e is the actual extrusion width, e' is the designed extrusion width, h is the layer height, and d is the diameter of the nozzle.

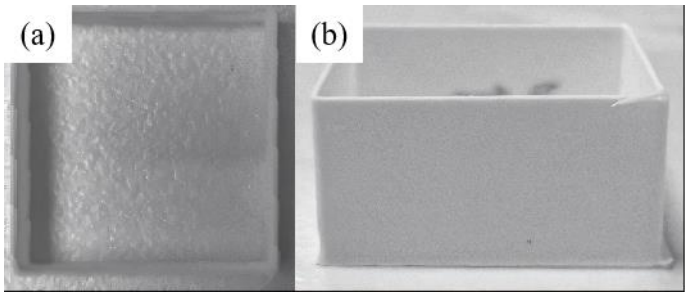

Figure 10 Lidless-Single-Wall Cubes (LSC) model: (a) top view; (b) front view.

After calculating the A_e, the actual printed volume per second is compared with the designed volume, and the volume expansion ratio is calculated as the ratio of the actual volume to the designed volume. The appropriate flow multiplier is then derived using the volume expansion ratio, thereby determining the initial flow multiplier. The detailed derivation

of the volume expansion ratio and flow multiplier calculation process will be presented using the relevant formulas:

$$V_A = A_e * P_s \tag{3}$$

$$V_D = A'_e * P_s \tag{4}$$

$$VER = \frac{V_A}{V_D} \tag{5}$$

Where P_s is the print speed, V_A is the actual printed volume per second, V_D is the designed printed volume per second, and VER is the Volume Expansion Ratio.

The VER reveals that at a 90% flow multiplier, the V_A exceeds the V_D. By appropriately reducing the flow multiplier, the actual value can be aligned with the designed value, thereby improving printing accuracy and consistency. Next, the initial flow multiplier will be calculated using the relevant formula to adjust the deviation between the V_A and V_D:

$$V' = \frac{V_A - V_D}{V_D} * 100\% \tag{6}$$

$$f_c = \frac{f_i}{1 + V'} * 100\% \tag{7}$$

Where V' is the percentage increase from V_D to V_A, f_c is the initial calibrated flow multiplier, and f_i is the initial flow multiplier.

Taking foaming PLA fabricated at $250°C$ nozzle temperature as an example, the value of major variables from the equations (1)-(7) are presented in the Table 3 below.

Table 3 Calculation of extrusion width, area and volume.

Name	e	A_e	A'_e	V_A
LSC	$1.07\ mm$	$0.179\ mm^2$	$0.044\ mm^3$	$4.475\ mm^3$
Name	V_D	VER	V'	f_c
LSC	$1.142\ mm^3$	3.918	291.8%	22.97%

After calculating the initial calculated flow multiplier, it needs to be validated. The LSC model is used for printing and measurement of e. These measurements are then compared with the e' to determine if they are equal. If they are not equal, the following formula is applied for fine-tuning to further optimize the f:

$$f = \frac{e'}{e} * 100\% \quad (8)$$

Where f is the calibrated flow multiplier.

The flow chart calibration process is illustrated in the Figure 12. Based on the calibration process outlined in this section, calibration was performed for nozzle temperatures of $210℃$, $230℃$, and $250℃$. The calibrated extrusion width is measured as shown in Figure 11. To determine the extrusion width for each LSC structure, measurements were taken at four separate wall positions, with the final reported value being their mean value. Statistical evaluation via one-way ANOVA produced a P-value of 0.31, demonstrating that variations in nozzle temperature do not significantly affect extrusion width. And calibrated flow multiplier will be presented in Table 4.

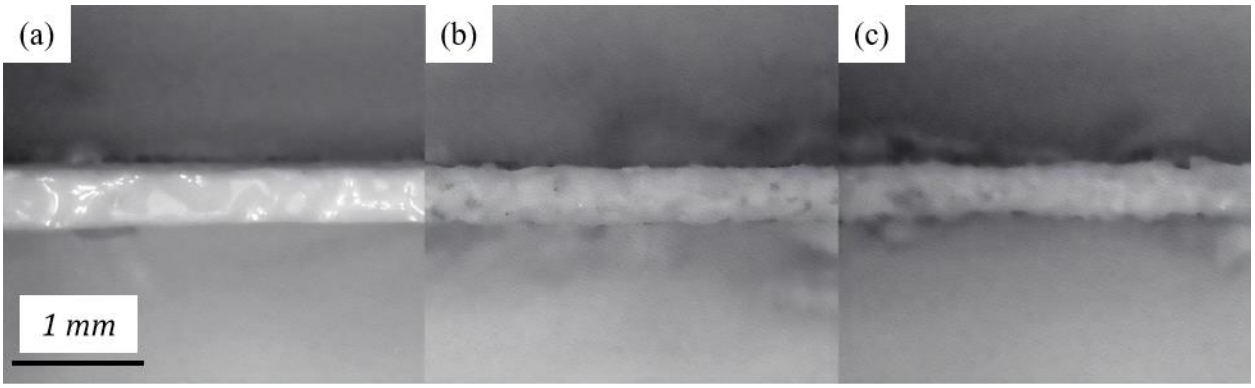

Figure 11 Calibration results of foaming PLA extrusion width (0.4 mm) under nozzle temperatures at (a)210˚C, (b)230˚C; (c)250˚C.

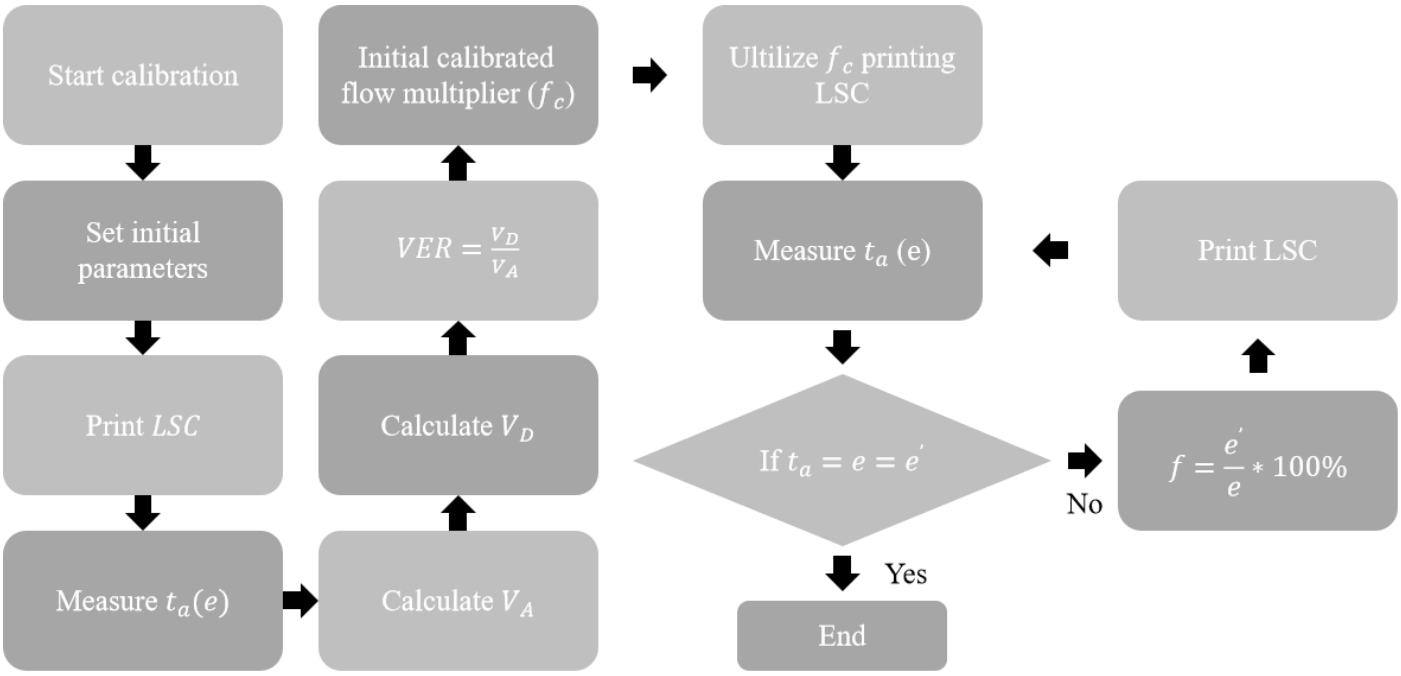

Figure 12 The flow chart of calibration process.

3.3 Impacts of Fabrication Process Parameters on Porosity and Densities of Foaming PLA and PLA Materials

In this research, three different nozzle temperatures (210℃, 230℃ and 250℃) were applied to print foaming PLA, as the nozzle temperature affects its porosity and density. Besides porosity, nozzle temperature also affects the filament extrusion width if the filament extrusion speed keeps constant, since the materials have different expansion ratios under different nozzle temperatures. In this work, we kept the filament extrusion width (0.4 mm) as a constant by calibrate the extrusion speed. Specifically, a flow multiplier defined as a ratio between the extrusion speed of foaming PLA and the extrusion speed of PLA that can achieve the same extrusion width was used. This ratio has been calibrated based on the approach summarized in the previous chapter. The calibrated ratio, porosity and bulk density of foaming PLA base material at different nozzle temperatures are summarized in Table 4.

Table 4 The calibrated ratio, porosity, and bulk density of foaming PLA base material under different nozzle temperatures.

	Nozzle temperature [℃]	Calibrated ratio	Porosity [%]	Measured bulk density [g/cm^3]
Foaming PLA	210	0.642	40.8	0.71

230	0.343	68.6	0.38
250	0.291	73.3	0.32

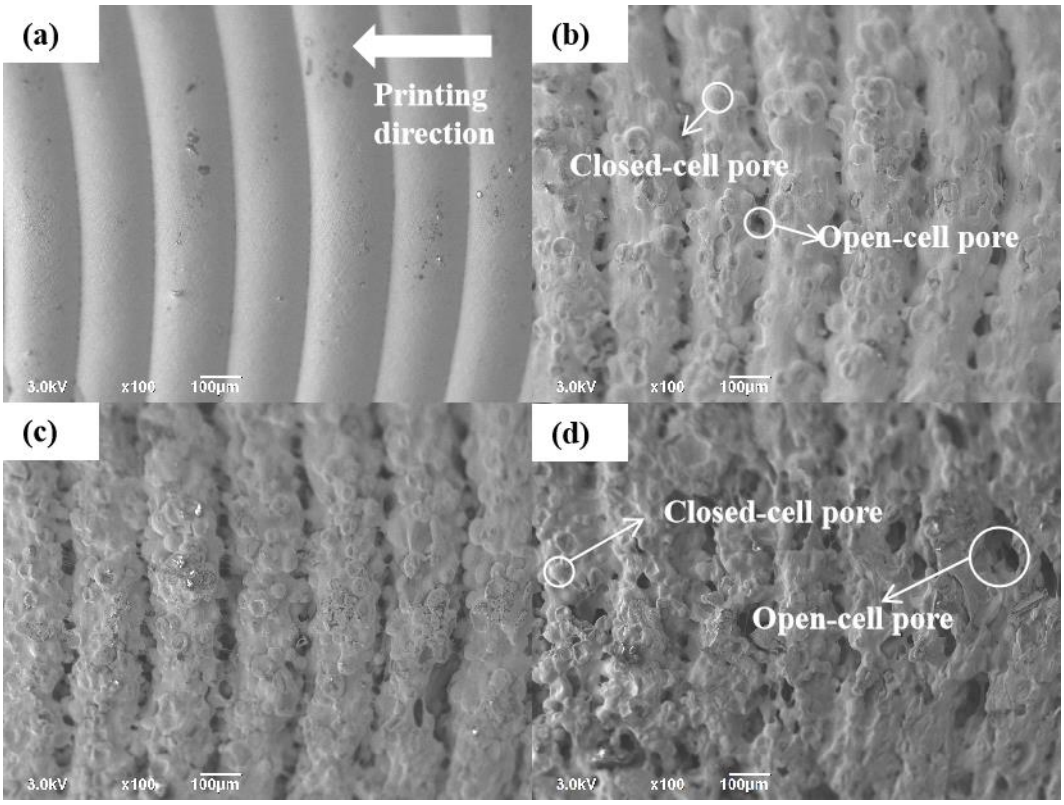

Figure 13 SEM images of (a) PLA; Foaming PLA fabricated at (b) 210℃; (c) at 230℃ and (d) at 250℃.

To further investigate the impacts of nozzle temperatures on pores morphologies on microscale, SEM (Scanning Electron Microscopy) has been applied to examine the surface of printed samples, and their results are presented in Figure 13. Compared to foaming PLA materials, the surface of non-foaming PLA materials, as shown in Figure 13(a), is smooth without any pores or bubbles. However, the obvious layer lines can be observed perpendicular to the printing direction. Under 210℃ nozzle temperature, many closed-cell pores can be identified. These pores lead to a rough boundary between layers where some open-cell pores can be identified as shown in Figure 13(b). When the nozzle temperature further increased for foaming PLA materials, the pore size increased, and a few closed-cell pores started to transfer to open-cell pores as shown in Figure 13(c). In addition, the size of open-cell pores along the layer boundary are keep increasing compared to foaming PLA materials printed under 210℃ nozzle temperature. When the nozzle temperature reaches 250℃ as shown in Figure 13(d), the boundary between layers can be hardly identified due to the large open-cell pores are randomly distributed on both layer boundaries and inside each layer. Due to the high

temperature, materials have better flowability since the air gap due to lack of fusion cannot be found under this temperature. In addition to open-cell pores, we can still identify a few closed-cell pores. Thus, under 250℃ nozzle temperature, the printed foaming PLA material has mixed open and closed-cell pores. The impacts of those pore morphologies and bounding quality will also affect the mechanical properties of printed foaming PLA materials which will be discussed in the next sub-section.

3.4 Impacts of Fabrication Process Parameters on Mechanical Properties of Foaming PLA and PLA Materials

To further understand how the nozzle temperature will affect the mechanical properties of fabricated foaming materials, unidirectional tensile tests and compressive testing have been done on PLA samples as well as foaming PLA samples were characterized by the standard of test procedure ASTM D638 and ASTM D695, respectively. The printing orientation of those samples are shown in Figure 14.

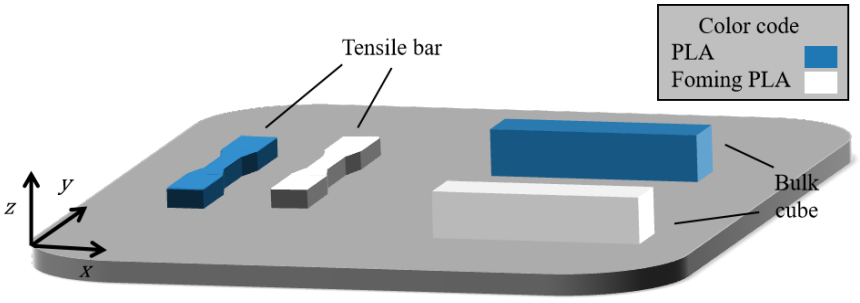

Figure 14 Schematics of the 3D printed samples for tensile and compressive testing, showing the printing orientation (Z) with respect to the printing bed.

Strain-stress curves of PLA and foaming PLA materials are illustrated in Figure 15(a). Compared to the results reported from the previous research [161], the measured stress-strain curve of PLA material shows similar trends specifically similar tensile elastic modulus, tensile yield strength. and elongation as shown in Table 5. Comparing to PLA materials, the foaming PLA materials show less elastic modulus and yield strength due to their porosity. But foaming PLA materials, specifically for those materials fabricated under 210℃, show a better elongation compared to PLA.This is due to the closed-cell pores induced by the foaming agents. These closed-cell pores increase the elongation of the materials because

the interactions among the cell walls allow for a more uniform stress distribution. As a result, the material can maintain high elongation under high strain conditions, a working mechanism that explains this behavior has been previously discussed [162]. Comparing to the foaming materials fabricated under 210℃, those materials fabricated under 230℃, more open-cell pores on the surface and the bonding between layers will likely initiate small cracks and cause the brittle failure in the earlier stage. That is the reason why samples printed at 230℃ shows the lowest elongation. As to temperature further increases, the better bonding has achieved which can enhance its elongation but due to the open-cell pores along the boundaries, it still cannot achieve the same elongation as sample at 210℃.

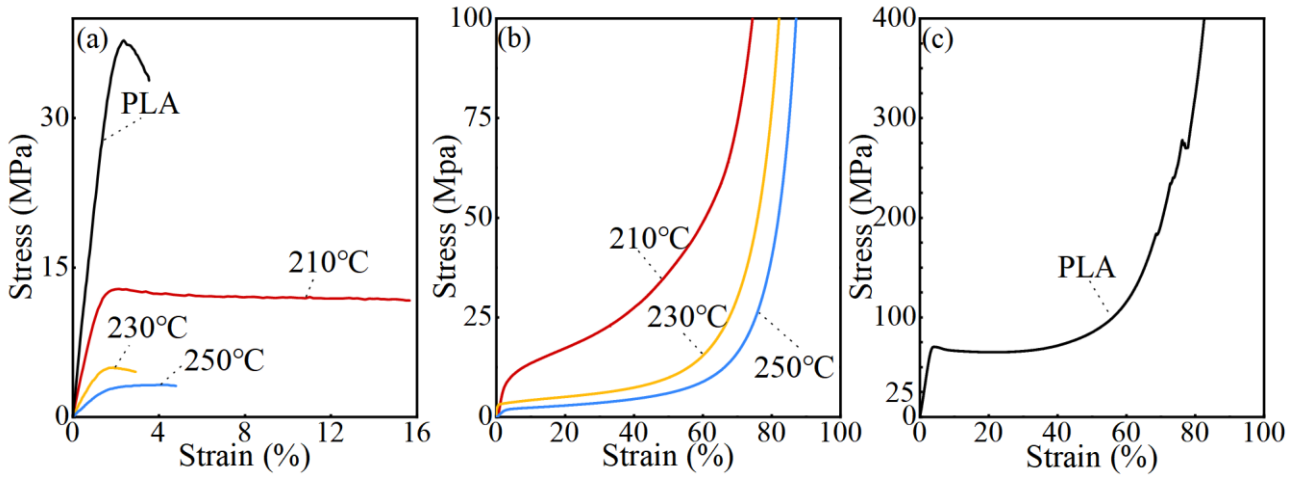

Figure 15 (a) The stress-strain curves of tensile tests for PLA and foaming PLA materials fabricated at 210℃, 230℃ and 250℃ nozzle temperatures; (b) the stress-strain curves of compression tests for foaming PLA materials fabricated at 210℃, 230℃ and 250℃ nozzle temperatures and (c) the stress-strain curves of compression test for PLA materials.

In addition to tensile tests, compression tests were performed to print PLA and foaming PLA materials. Figure 15(b) and (c) show the stress-strain curves of PLA and foaming PLA materials. Compared to PLA materials, foaming PLA materials show much lower elastic modulus and yield strength. Also, the compressive elastic moduli and yield strength of foaming PLA materials under different nozzle temperatures are lower than that from tensile tests. The reason for this is that the wall of pores in foams is more likely to fracture under compressive loading conditions [163].

To further compare the mechanical properties of the materials based on their density, the specific modulus, yield strength, and toughness are calculated based on the tensile stress-strain curves shown in Figure 15(a). The results are tabulated in Table 5.

Specific modulus (S) can be calculated as follows:

$$S = \frac{E}{\rho} \tag{9}$$

Where E is elastic modulus of materials or honeycomb structures, and ρ is the density of materials or honeycombs.

Table 5 The specific modulus, yield strength and toughness of PLA and foaming PLA materials from tensile tests.

	PLA	Foaming PLA		
		210℃	230℃	250℃
Specific modulus [Mpa · m]	1.86	0.61	0.45	0.25
Yield strength [Mpa]	35.4	11.6	4.6	2.71
Toughness [J/m^3]	9.67×10^7	1.82×10^8	1.1×10^7	1.24×10^7

It should be noted that PLA materials exhibit the highest specific modulus among materials, demonstrating superior rigidity and strength. In contrast, foaming PLA materials have a lower specific modulus, exhibiting lower stiffness and bending resistance with respect to weight. Experimental results indicate that increasing nozzle temperatures cannot enhance foaming PLA materials' specific modulus. However, when the nozzle temperature reaches 210℃, it presents the longest elongation and highest toughness among materials. This finding suggests that although foaming PLA materials have lower rigidity, they possess good energy absorption capacity and deformation ability. By combining PLA and foaming PLA materials, their respective advantages can be leveraged. The PLA 'skins' provide high stiffness to prevent structural deformation, while the foaming PLA 'cores' improve energy absorption capabilities. This combination shows great potential, especially in hierarchical honeycomb structures that utilize both materials. The details of the design of hierarchical materials will be discussed in Chapter 4.

3.5 Summary

In other words, the extrusion width of foaming PLA has to be calibrated to make sure the FFF process has dimensional accuracy. The flow multiplier can be changed with respect to the nozzle temperature to precisely control the extrusion width to match the designed dimensions. This calibration method addresses the expansion caused by the foaming agent in the material, which can affect the actual printed volume. In a few iterations, the flow multiplier will be adjusted to

make the extruded width consistent at a different temperature, and the optimized parameters obtained will be used for printing the base material to conduct the base material mechanical test.

The next chapter will explore how the calibrated extrusion process for foaming PLA can be combined with the innovative use of both PLA and foaming PLA materials to construct honeycomb structures with superior mechanical properties and energy absorption capabilities.

Chapter 4: Design and fabrication of hierarchical honeycomb structures

This chapter will introduce the process of design and fabrication of hierarchical honeycomb structures. Section 4.1 will present the overall procedure of design and fabrication for hierarchical honeycomb structures. Section 4.2 proposes a design of unit cells. Section 4.3 and 4.4 introduce the multi-scale design of hierarchical honeycomb structures and experiments, respectively. Section 4.5 presents the fabrication results.

4.1 Unit Cells Multi-Scale Design

The design of proposed honeycomb structures is shown in Figure 16, which contains three design scales. On macroscale, hexagonal honeycomb with internal angle θ = 120° and cell length L = 9 mm was designed. Its wall thickness can be controlled to achieve different macroscale relative density ρ_h^* of honeycomb. The following equation was used [164]:

$$\rho_h^* = \frac{2\mathrm{t}}{\sqrt{3}l} \tag{10}$$

On mesoscale, specifically for each wall of honeycomb, t_s/t_f which is defined as a ratio between the thickness of skin layers t_s and foam layers t_f, can be further tailored. On microscale, the relative density of foaming PLA (ρ_f^*) can be tuned by adjusting nozzle temperatures. The combination of microscale and mesoscale features can control the relative density of the sandwich wall that was calculated by the equation:

$$\rho_{sa}^* = \frac{t_f\rho_f^* + 2t_s}{2t_s + t_f} \tag{11}$$

where, ρ_{sa}^* refers to the relative density of sandwich panel. t_f is the thickness of foam layer and t_s is the thickness of skin layers as illustrated on Figure 16(f). The overall relative density of the designed hierarchical honeycomb structures can be calculated:

$$\rho^* = \rho_h^*\rho_{sa}^* \tag{12}$$

where, $\rho^*$is total relative density of honeycomb. ρ_h^* refers to the honeycomb structure and ρ_{sa}^* is the relative density

of the sandwich panel.

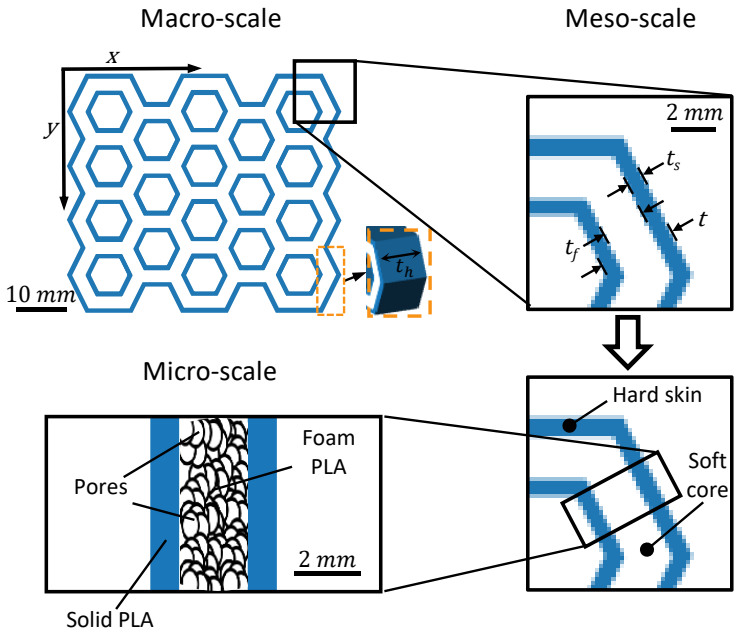

Figure 16 Hierarchical honeycomb structures design.

4.2 Fabrication of Hierarchical Honeycomb Structures

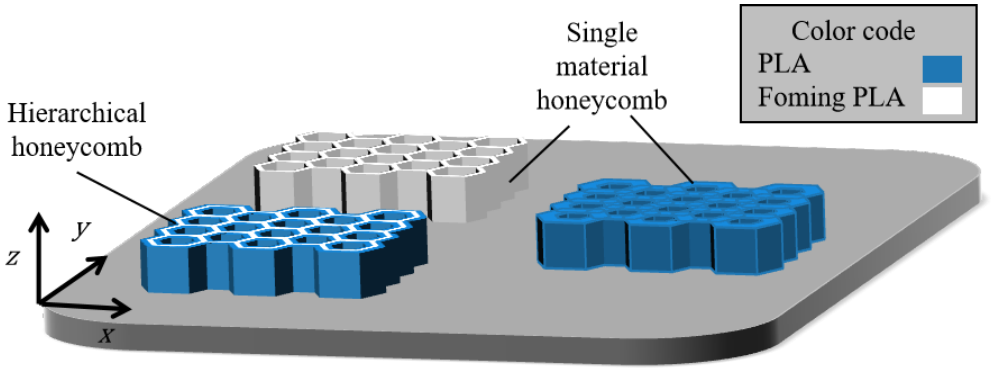

Figure 17 Schematics of the 3D printed samples of honeycomb structures, showing the printing orientation with respect to the printing bed and Z is printing direction.

To fabricate the designed samples, a multi-material extrusion machine Bambu Lab X1C was used to fabricate the designed samples the reasons have been explained in Chapter 3. The printing orientations of designed samples are shown in Figure 17. As to the printing parameters, the same process parameters discussed in Chapter 3 are used while the nozzle

temperature are controlled to achieve the different porosity of foaming materials.

Based on the printed models, no significant differences in Z-direction height were observed between foam PLA and solid PLA honeycombs. Moreover, due to the hierarchical honeycomb design and its printing orientation, the two materials are not stacked on top of each other along the Z-axis. In other words, foam PLA layers are printed consecutively on foam PLA, and solid PLA layers are printed consecutively on solid PLA. As a result, there is no risk of nozzle collision with the printed structures during the printing process.

4.3 Printing Experiment Setup

A honeycomb structure with $5 * 4$-unit cells was designed for uniaxial compression test and illustrated in Figure 16(a). The thickness of this honeycomb structures Z is $20\ mm$ to avoid its out-plane buckling or instability along the Z-axis during compression testing. To investigate how the design parameters discussed in section 4.1 including t_s, t_f and nozzle temperature affect the compression behaviors of hierarchical honeycomb structures, a set of experiment has been designed and summarized in Table 6. Specifically, in the baseline model, $t_s = 0.4\ mm$ and $t_f = 2\ mm$ which means there are 1 layer of skin and 5 layers of foaming core. To change the relative density of designed honeycomb structures, we can either increase the number of layers for skin or varying the number of layers for core. By increasing the number of layers for skin, the t_s/t_f ratio 2/5 and 3/5 can be achieved. By changing the number of layers for core, the t_s/t_f ratio 1/2 and 1/10 can be fabricated. For each ratio, three different nozzle temperatures: $210℃$ $230℃$ and $250℃$ are going to be used. In total, 15 groups of samples will be fabricated. Each group will contain 3 samples to verify the repeatability of the experiment.

Table 6 Design of hierarchical honeycombs with various t_s/t_f ratio

Experiment group	t_s $[mm]$	t_f $[mm]$	Nozzle temperature [℃]	Nominal relative density [-]
210H 1/5 (210H-1-5)	0.4	2.0	210	0.239
210H 2/5 (210H-2-5)	0.8	2.0	210	0.321
210H 3/5 (210H-3-5)	1.2	2.0	210	0.394
230H 1/5 (230H-1-5)	0.4	2.0	230	0.171
230H 2/5 (230H-2-5)	0.8	2.0	230	0.254

230H 3/5 $_{(230H-3-5)}$	1.2	2.0	230	0.329
250H 1/5 $_{(250H-1-5)}$	0.4	2.0	250	0.159
250H 2/5 $_{(250H-2-5)}$	0.8	2.0	250	0.242
250H 3/5 $_{(250H-3-5)}$	1.2	2.0	250	0.317
210H 1/2 $_{(210H-1-2)}$	0.4	0.8	210	0.165
210H 1/10 $_{(220H-1-10)}$	0.4	4.0	210	0.342
230H 1/2 $_{(230H-1-2)}$	0.4	0.8	230	0.135
230H 1/10 $_{(230H-1-10)}$	0.4	4.0	230	0.219
250H 1/2 $_{(250H-1-2)}$	0.4	0.8	250	0.130
250H 1/10 $_{(250H-1-10)}$	0.4	4.0	250	0.197

In addition to those honeycomb structures designed with mixed foam PLA and solid PLA, the honeycomb structure with pure material which is either PLA or foaming PLA are also fabricated as a comparison group. Their design parameters are summarized in Table 7.

Table 7 Control group of pure material (foaming PLA or PLA) honeycombs.

	Foaming PLA			PLA
Nozzle temperature [℃]	210	230	250	190
Relative density [-]	$RD = 0.1_{(210F\ 0.1)}$ $RD = 0.2_{(210F\ 0.2)}$ $RD = 0.3_{(210F\ 0.3)}$	$RD = 0.1_{(230F\ 0.1)}$ $RD = 0.2_{(230F\ 0.2)}$ $RD = 0.3_{(230F\ 0.3)}$	$RD = 0.1_{(250F\ 0.1)}$ $RD = 0.2_{(250F\ 0.2)}$ $RD = 0.3_{(250F\ 0.3)}$	$RD = 0.1_{(P\ 0.1)}$ $RD = 0.2_{(P\ 0.2)}$ $RD = 0.3_{(P\ 0.3)}$

4.4 Fabrication Results

In total 27 different honeycomb structures have been designed in Section 4.4. Three samples will be fabricated and tested for each design. In total, 81 samples have been successfully fabricated. The fabricated sample for

In total 81 honeycomb samples have been successfully fabricated. Some successfully fabricated samples are shown in Figure 18. Before the mechanical testing of these samples, the dimension and relative density of samples are measured via vinier caliper and balance ($10mg$) and their results are summarized in Table 8.

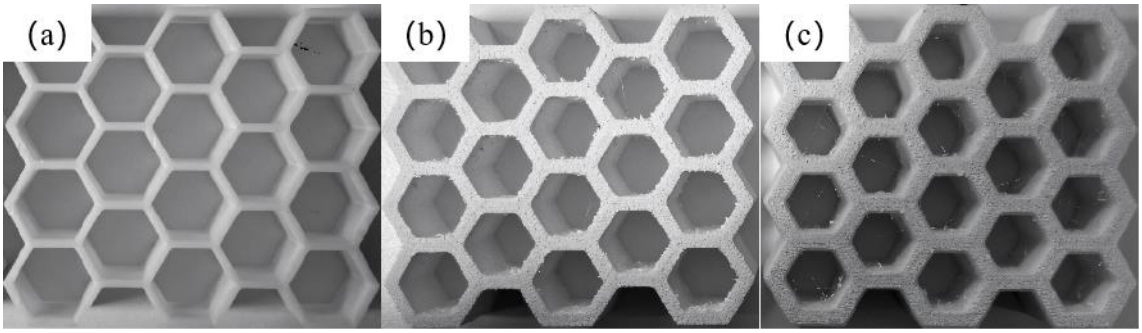

Figure 18 Representative fabricated samples: (a) honeycomb structure with pure solid PLA; (b) honeycomb structure made of pure foaming PLA; (c) Hierarchical honeycomb structures with solid PLA skin and foaming PLA cores.

Table 8 Details of the hierarchical honeycomb structures studied in this research.

Experiment group	Nozzle temperature [℃]	Measured relative density [-]	Measured thickness $[mm]$
210H-1-5	210	0.224 ± 0.000	2.81 ± 0.02
210H-2-5	210	0.286 ± 0.001	3.60 ± 0.01
210H-3-5	210	0.369 ± 0.002	4.43 ± 0.01
230H-1-5	230	0.175 ± 0.001	2.80 ± 0.01
230H-2-5	230	0.245 ± 0.002	3.60 ± 0.01
230H-3-5	230	0.322 ± 0.000	4.41 ± 0.01
250H-1-5	250	0.161 ± 0.001	2.81 ± 0.02
250H-2-5	250	0.235 ± 0.002	3.62 ± 0.01
250H-3-5	250	0.308 ± 0.003	4.41 ± 0.01
210H-1-2	210	0.165 ± 0.002	1.60 ± 0.02
220H-1-10	210	0.379 ± 0.003	4.82 ± 0.01
230H-1-2	230	0.135 ± 0.002	1.62 ± 0.01
230H-1-10	230	0.235 ± 0.002	4.82 ± 0.01
250H-1-2	250	0.129 ± 0.001	1.60 ± 0.01
250H-1-10	250	0.217 ± 0.000	4.82 ± 0.01
P 0.1	190	0.106 ± 0.000	0.82 ± 0.02
P 0.2	190	0.217 ± 0.000	1.70 ± 0.02

P 0.3	190	0.311 ± 0.002	2.54 ± 0.01
210F 0.1	210	0.108 ± 0.001	1.30 ± 0.01
210F 0.2	210	0.203 ± 0.002	2.55 ± 0.01
210F 0.3	210	0.292 ± 0.000	3.85 ± 0.01
230F 0.1	230	0.103 ± 0.001	2.51 ± 0.01
230F 0.2	230	0.1848 ± 0.002	4.94 ± 0.01
230F 0.3	230	0.256 ± 0.002	7.35 ± 0.01
250F 0.1	250	0.099 ± 0.002	2.91 ± 0.01
250F 0.2	250	0.169 ± 0.000	5.82 ± 0.01
250F 0.3	250	0.239 ± 0.000	8.81 ± 0.01

The measurement results revealed that in foaming PLA honeycomb structures, there was a noticeable discrepancy between the measured relative density and the designed relative density. The discrepancy arises from the use of Ashby's relative density equation (10), which is based on the thin-wall assumption for initial calculations. This equation provides a simplified approximation of the relationship between relative density, wall thickness, and arm length for honeycomb structures, and is particularly suited for structural design under the thin-wall assumption [165]. When wall thickness is large, this equation may lead to errors in predicting relative density, as it does not fully account for node effects, three-dimensional stress distribution, and nonlinear changes in material volume in thick-walled hexagonal honeycomb structures [166]. These factors contribute to the differences between the design calculations and the actual measurements. However, the focus of the results in next chapter is not on the absolute precision of the density values, but rather on the influence of t_s/t_f ratios and nozzle temperatures on the honeycomb structures and its mechanical properties.

4.5 Summary

The chapter focuses on the design and fabrication of hierarchical honeycomb structures. The current section first introduces the design methodologies for unit cell and hierarchical configuration with an emphasis on the role of the different scales—macroscale, mesoscale, and microscale—on the final properties of the structures. In this section, some mechanical performances for the discussed hierarchical designs will be outlined, considering compression testing activities to understand both material distribution and fabrication parameters' relationships to mechanical properties,

such as elastic modulus, initial peak stress, and energy absorption.

Chapter 5: Mechanical Testing of Hierarchical Honeycomb Structures

To evaluate the mechanical properties of hierarchical honeycomb structures, the unidirectional compressive tests have been done. This chapter will detail the experiments' procedures and results. Section 5.1 will introduce the detailed compressive testing setup of hierarchical honeycomb structures. Section 5.2 introduces the finite element analyze (FEA) setup. Section 5.3 analyzes the stress-strain curve behavior of honeycomb structures. Section 5.4 evaluates the mechanical properties of honeycomb structures. Section 5.5 provides a discussion for the honeycomb structures' results.

5.1 Compressive Testing Setup

To investigate the effects of design parameters on the mechanical performance of hierarchical honeycomb structures, a standard unidirectional compression test setup based on ASTM C365 has been used. The loading rate of $2\ \mathrm{mm/min}$ is selected to evaluate the quasi-static compressive behavior of honeycomb structures. Figure 19 illustrates an experiment setup with a hierarchical honeycomb structure positioned between the compression plates.

Figure 19 Setup of unidirectional compression test for a fabricated honeycomb sample.

5.2 Calculation of Mechanical Properties

The mechanical properties of the tested structures were extracted from stress-strain data obtained from the compressive test discussed in Section 5.1. Specifically, the compressive modulus was calculated based as the slope of the linear elastic section; initial peak stress was calculated as the value of first peak stress. The capacity for energy absorption in cellular solids, defined as the energy absorbed per unit volume, corresponds to the area under the stress-strain curve up to the point of densification strain.

$$W = \int_0^{\varepsilon_D} \sigma(\varepsilon) d\varepsilon \tag{13}$$

where the densification strain, denoted as ε_D, was determined using the energy absorption efficiency method, which identifies the onset of densification at the strain value $\sigma(\varepsilon)$ where maximum efficiency occurs, the equation is given [167]:

$$\eta(\varepsilon_D) = \frac{\int_0^{\varepsilon_D} \sigma(\varepsilon) d\varepsilon}{\sigma(\varepsilon)_{\varepsilon=\varepsilon_D}} \tag{14}$$

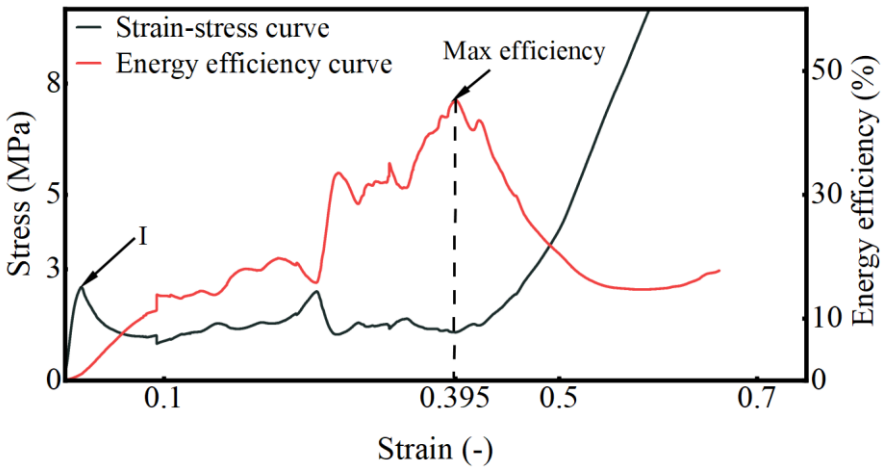

Figure 20 Strain-stress and energy efficiency curves of 210H 1-10 hierarchical honeycomb structures.

And corresponding strain becomes the densification strain if the curve of energy absorption efficiency reaches the max, the equation of which is given by:

$$\frac{d\eta(\varepsilon)}{d\varepsilon}|_{\varepsilon=\varepsilon_D} = 0 \tag{15}$$

This approach is favored for characterizing the densification behavior of cellular materials, owing to its consistency and reliability [167][168]. An illustration of this is provided in Figure 20. Point I marks the initial peak stress (σ_p) in the Figure 20 as well.

5.3 Finite Element Modeling

To further explain the experimental results, this research also employed numerical analysis tool, specifically finite element simulation, to analyze the differences in stress distribution between hierarchical honeycomb structures and single-material honeycomb structures. The simulation aimed to reveal how the hierarchical design alters stress concentration locations and distribution characteristics, thereby validating its effectiveness in optimizing mechanical performance.

The numerical simulation of the honeycomb structures was conducted with the commercial FE package *Abaqus/Explicit 2021*, aiming to capture the compressive response of structures. *Abaqus/Explicit* was chosen for its capability to handle highly nonlinear problems such as large deformations and buckling, making it well-suited for the complex deformation and failure behavior of foaming PLA under loading. Additionally, it efficiently manages contact interactions between rigid rods and the honeycomb structure, avoiding the convergence issues associated with implicit solvers. The step-by-step solution approach addresses local failures and stress concentration effectively. Since explicit solvers do not require iterative calculations, they are ideal for simulating loading processes over short durations [169][170][171].The base material PLA and foaming PLA were modeled with linear elastic properties. To achieve consistent element sizing at the joints of the hierarchical honeycomb unit cell, construction lines were incorporated in the Abaqus sketch, guiding the meshing process to maintain uniform grid distribution at these critical regions (as shown in Figure 21(a)). The geometry and boundary conditions of each test were exactly adapted in the corresponding FE simulations. Mesh-independence of each model was verified by mesh convergence analysis. To apply the displacement boundary condition in the U_2 direction, two rigid bars were introduced in the model as boundary constraints (as shown in Figure 21(b)). One side was fully fixed, while a specified displacement was applied to the other side to simulate the structural response under loading in that direction. Contact between the rigid bars and the structure was defined as frictionless to simplify the simulation. The honeycomb structure, designed in a two-dimensional plane and extruded along the out-of-plane

direction, was modeled using a 2D planar model with a thickness assigned to approximate three-dimensional mechanical behavior. Honeycomb structures were modeled with 4-node continuum plane stress quadrilateral elements (CPS3).

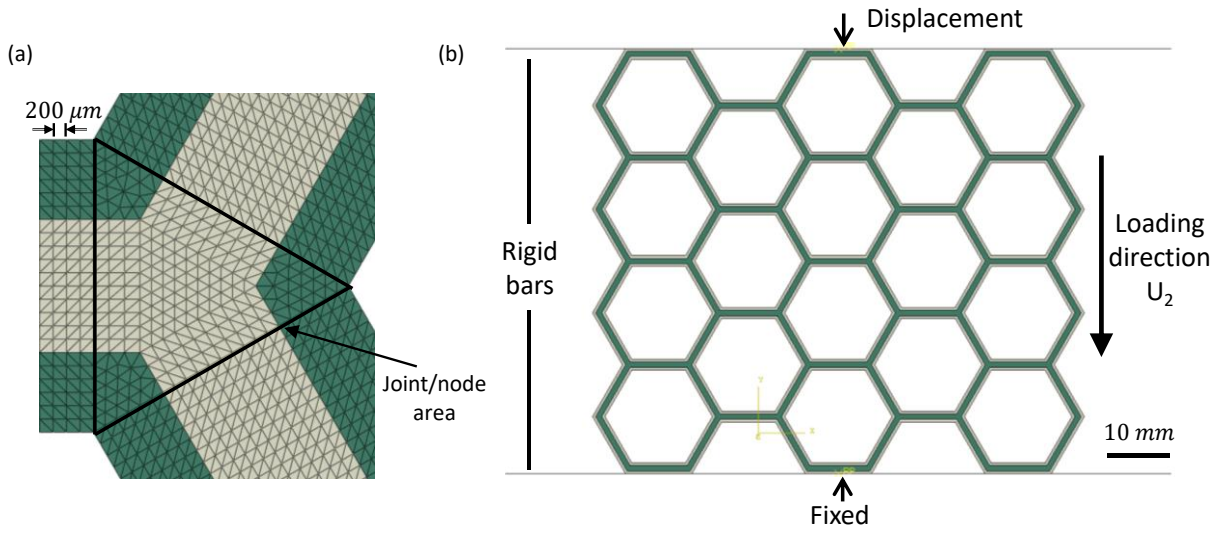

Figure 21 (a) Utilizing addition lines on Joint/node area for uniform meshing; (b)boundary condition of simulation model.

5.4 Compressive testing results

5.4.1 Compressive testing results of pure PLA and foaming PLA honeycombs

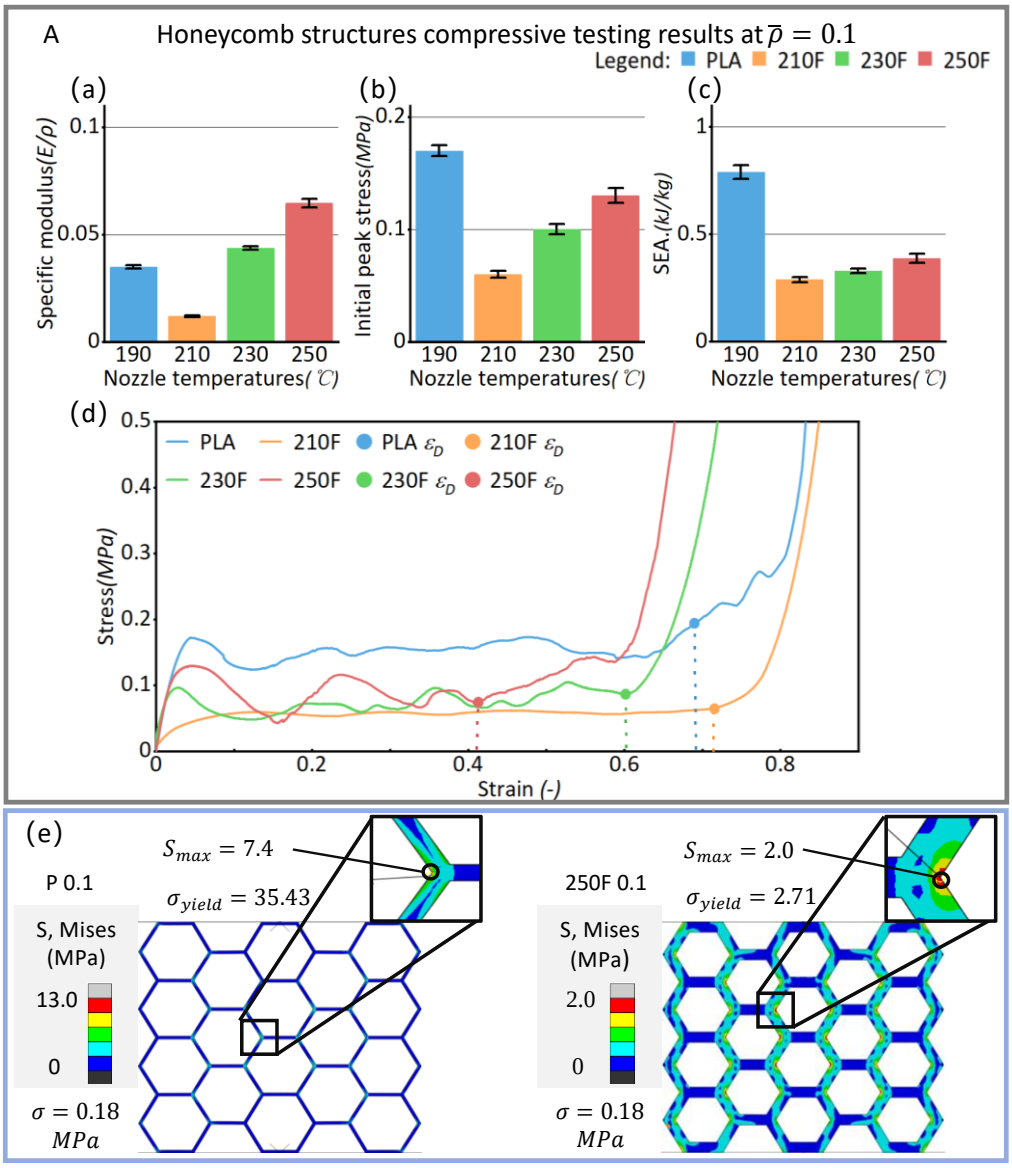

Figure 22 Results of pure PLA and foaming PLA honeycomb structures with nominal relative density of 0.1. (a) Specific modulus of pure PLA and foaming PLA at nominal relative density of 0.1; (b) Initial peak stress of pure PLA and foaming PLA at nominal relative density of 0.1; (c) Specific energy absorption (SEA.) of pure PLA and foaming PLA at nominal relative density of 0.1; (d) Strain-stress curves of pure PLA and foaming PLA at nominal relative density of 0.1 and dotted lines indicate densification strain; (e) The max. Von mises position and value of P 0.1 and $250F$ 0.1captured by Abaqus.

The unidirectional compression tests for all the 81 samples have been successfully done. Among those 81 samples, the

results of honeycomb structures made of pure PLA and foaming materials under different nozzle temperatures are summarized in Figure 3. The designed relative density of these honeycomb structures is all the same and equal to 0.1.

Although solid PLA and foaming PLA honeycomb structures were designed with the same relative density, variations in actual relative density were observed due to the printing process (as shown in Table 8 from Section 5.3). To ensure a fair comparison of structural performance, this research employed the specific modulus method, normalizing the compressive modulus of the structures by their respective densities:

$$S = \frac{E_h}{\rho} \tag{16}$$

Where S is the specific modulus of honeycomb, E_h is the compressive modulus of honeycomb, and ρ is the density of the honeycomb.

As it is shown in Figure 3(a), the specific modulus of foaming PLA is lower than that of solid PLA at nozzle temperatures of $210°C$. However, as the nozzle temperature increases, the specific modulus shows an overall upward trend, with a significant improvement observed at $250°C$. Specifically, the specific modulus of the foaming PLA honeycomb structure at $250°C$ exceeds that of solid PLA, primarily because the wall thickness ($t = 2.92mm$) of foaming PLA is significantly greater than that of solid PLA ($t = 0.78mm$), thereby greatly enhancing the flexural modulus of honeycomb walls. Even high foaming ratio will lead to the decrease of its elastic modulus; however, the increase of wall thickness has a higher impact.

This trend can be explained by the bending stiffness of the beams. Beams with higher bending stiffness are less prone to bending deformation under compressive loads, enhancing the overall compressive resistance of the honeycomb structure, as reflected in a higher compressive modulus. The bending stiffness (D) formula used for this analysis is as follows:

$$D = \frac{48 * E_s * I}{L^3} \tag{17}$$

Where E_s is the Young's modulus of pure PLA and foaming PLA which are obtained from tensile test in section 5.3, L is the length of the cell wall ($9mm$ in this research), and I is the second moment of area of inertia of the cell wall. for a wall of uniform thickness:

$$I = \frac{1}{12} * b * t^3 \tag{18}$$

Where b is the width of the cross section, $b = 20mm$ in this research, and t is the thickness of the honeycomb cell wall:

$$D = \ 4 * E_s * b * (\frac{t}{L})^{\ 3} \tag{19}$$

According to the tensile test results of base materials in section 5.3, The relationship between the relative density of the base material and its Young's modulus can be expressed in a power-law form as:

$$E_s = 2.86 * (\rho^*)^{1.88} \tag{20}$$

Where E_s is the Young's modulus of the base material, and ρ^* is the relative density of the base material. To combine Equation 20 into Equation 19, the process is outlined:

$$D = \ 2.86 * (\rho^*)^{1.88} \ * 4 * b * (\frac{t}{L})^{\ 3} \tag{21}$$

The relationship for bending stiffness can be further simplified:

$$D \propto \ (\rho^*)^{1.88} * (\frac{t}{L})^{\ 3} \tag{22}$$

Due to the design strategy as mentioned in Chapter 4, at same relative density, the product of thickness (t), width (b), and relative density (ρ^*) equals to a constant C, thus:

$$\rho^* = \frac{C}{tb} \tag{23}$$

To combine Equation 23 into Equation 12, the process is outlined:

$$D \propto \left(\frac{C}{tb}\right)^{1.88} * \ (\frac{t}{L})^{\ 3} \tag{24}$$

Relative density decreases with increasing t, the impact of t dominates its relationship with stiffness. This explains why, for foaming PLA, although the base material's relative density decreases with increasing nozzle temperature, the wall thickness increases, leading to an increase in stiffness. Consequently, the compressive modulus also increases. Since the design density remains consistent, the specific modulus is higher. Even foaming honeycomb has lower Von-mises stress, its value is more closed to the yield stress of foaming materials compared to that made of solid PLA. This result indicates that solid PLA can withstand higher load-bearing capacity.

Additionally, as shown in Figure 22(c) which summarized the energy absorption capabilities of both solid PLA and foaming PLA under different nozzle temperatures. Honeycombs with solid PLA demonstrates the highest specific energy absorption value due to its higher plateau stress and densification strain as illustrated in Figure 22(d). As to foaming PLA, the energy absorption value increases significantly with rising nozzle temperature. This phenomenon can be attributed to the optimal combination of a higher initial peak stress and a larger densification strain required for efficient energy absorption. Specifically, even the honeycomb with 210°C foaming PLA has the highest densification strain, its overall energy absorption capacity is still lower than that with 250°C foaming PLA, which is mainly due to the lower plateau stress, as shown in Figure 22(d).

To further investigate the influence of relative density on mechanical properties of solid and foaming honeycomb structures, compressive experimental results for honeycomb structures with different designed relative densities are summarized in Figure 23.

Both specific moduli of solid PLA and foaming PLA honeycomb increase when the relative densities increase as shown in Figure 23. Due to the larger wall thickness, the foaming PLA samples exhibit higher specific modulus compared to its solid counterpart with the same relative density. The same trend can be observed in Figure (b) for peak stress. Peak stress of foaming honeycomb increases with respect to the growth of relative density but is still lower than its counterpart with solid PLA materials. When it comes to the specific energy absorption, in general the higher relative density can achieve higher specific energy absorption for both solid and foaming PLA. However, when the relative reaches 0.3, honeycombs with foaming PLA exhibits the better energy absorption capability compared to its solid PLA counterpart. This can be explained in the figure d. The higher nozzle temperature can increase the plateau stress of foaming PLA while also keep its higher densification strain compared to that of honeycomb with solid PLA materials.

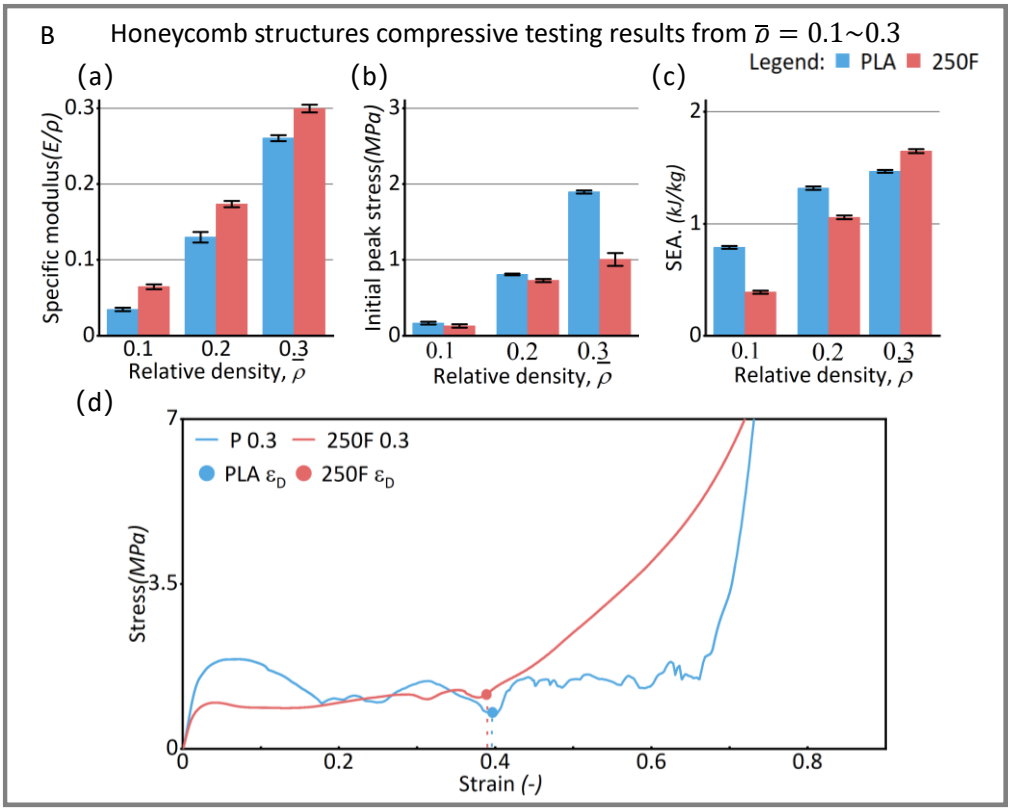

Figure 23 Results of pure PLA and foaming PLA (250℃) honeycomb structures with varying nominal relative density (0.1~0.3). (a) Specific modulus of pure PLA and foaming PLA (250℃) with varying nominal relative density (0.1~0.3); (b) Initial peak stress of pure PLA and foaming PLA (250℃) with varying nominal relative density (0.1~0.3); (c) Specific energy absorption (SEA.) of pure PLA and foaming PLA (250℃) with varying nominal relative density (0.1~0.3); (d) Strain-stress curves of pure PLA and foaming PLA (250℃) with varying nominal relative density (0.1~0.3) and dotted lines indicate densification strain.

Due to the larger wall thickness, the foaming PLA samples exhibit higher specific modulus compared to its solid counterpart with the same relative density. The same trend can be observed in Figure (b) for peak stress. Peak stress of foaming honeycomb increases with respect to the growth of relative density but is still lower than its counterpart with solid PLA materials. When it comes to the specific energy absorption, in general the higher relative density can achieve higher specific energy absorption for both solid and foaming PLA. However, when the relative reaches 0.3, honeycombs with foaming PLA exhibits the better energy absorption capability compared to its solid PLA counterpart. This can be explained in the Figure 23(d). The higher nozzle temperature can increase the plateau stress of foam PLA while maintaining a densification strain comparable to that of honeycomb structures made from solid PLA. Additionally, when

considering mass normalization, foam PLA exhibits a higher specific energy absorption (SEA) due to its lower density, despite having a similar densification strain.

5.4.2 Compressive testing results of hierarchical honeycombs

In order to understand the effects of two different design strategies on the mechanical properties of hierarchical honeycomb structures, the compressive test results of hieratical honeycomb structures with different foaming core thickness are presented and summarized in Figure 24. It is clear that specific modulus, initial peak stress, and SEA. are all increasing with respect to the increase of thickness of foaming core. The typical strain-stress curves for hieratical honeycomb with different core thickness are shown in Figure 24(b). Apparently, higher core thickness will lead to the decrease of densification strain but significantly increase the plateau stress. This is the major reason for its high energy absorption capacity.

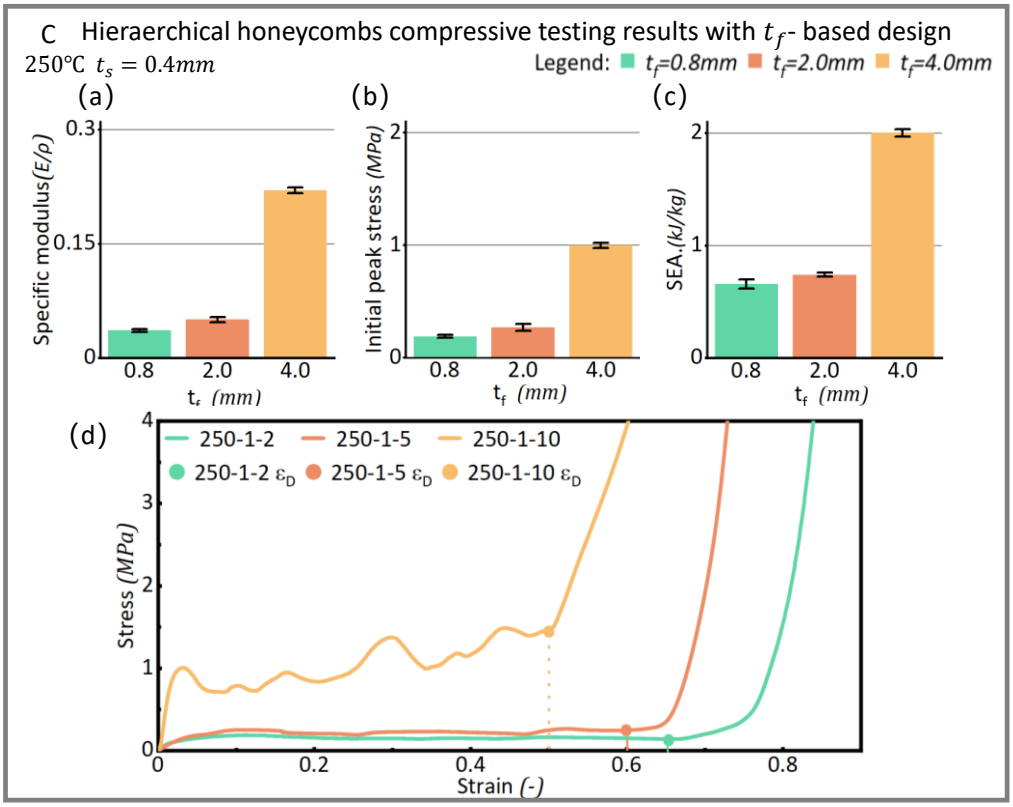

Figure 24 Results of hierarchical honeycomb structures with t_f ($t_f = 0.8, 2,$ and $4\ mm$) at different 250℃ nozzle temperatures. (a) Specific modulus of hierarchical honeycomb structures with t_f ($t_f = 0.8, 2,$ and $4\ mm$) at 250℃ nozzle temperatures; (b) Initial peak stress of hierarchical honeycomb structures with varying t_f ($t_f = 0.8, 2,$ and $4\ mm$) at 250℃ nozzle temperatures; (c) Specific energy absorption (SEA.) of hierarchical honeycomb structures with varying

t_f ($t_f = 0.8, 2,$ and $4\,mm$) at 250℃ nozzle temperatures; (d) Strain-stress curves of hierarchical honeycomb structures with varying t_f ($t_f = 0.8, 2,$ and $4\,mm$) at 250℃ nozzle temperature and dotted lines indicate densification strain.

Furthermore, the normalized compressive modulus E, initial peak stress σ_p, and the energy absorbed per unit volume W can each be represented as density-dependent power laws [164][172]:

$$\frac{E}{E_s} = C_1\overline{\rho}^{n_1} \tag{25}$$

$$\frac{\sigma_p}{\sigma_y} = C_2\overline{\rho}^{n_2} \tag{26}$$

$$\frac{W}{\sigma_y} = C_3\overline{\rho}^{n_3} \tag{27}$$

where E_s and σ_y represent the Young's modulus and yield strength of the base material (in this research, the properties of solid PLA are used), respectively. The coefficients C_1, C_2, C_3 and n_1, n_2, n_3 exponents coefficients describe the specific geometry of the unit cell. And the results are summarized in Figure 25. The small exponent of foaming PLA and solid PLA honeycomb structures means their compressive moduli reduce at a lower speed with decreasing relative densities, amplifying the advantages at low relative density ranges. However, compared to honeycomb structures made with pure solid and foaming PLA materials, at high relative density range, hierarchical honeycomb shows a better performance on effective elastic modulus, initial peak stress as well as energy absorption.

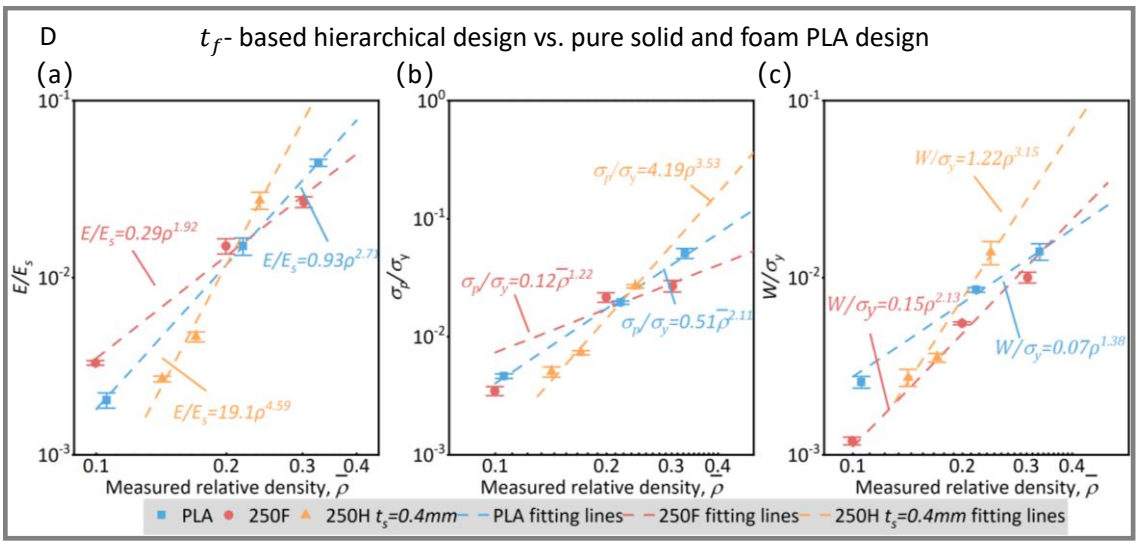

Figure 25 Normalized mechanical properties of foaming PLA, solid PLA honeycomb structures and hierarchical honeycomb tailoring with t_f along the in-plane direction with respect to the measured relative density: (a) elastic modulus, (b) initial peak stress, (c) energy per unit volume. Dashed lines indicate the best fitting lines of experimental data using power laws.

As to the second design strategy for the hierarchical honeycomb structures, the relative density of honeycomb structures in controlled by increasing the thickness of skint_s. The results of mechanical performance are summarized in Figure 26, Specific modulus, initial peak stress, and SEA. are all increasing with respect to the increase of thickness of solid skin. The typical strain-stress curves for hieratical honeycomb with different skin thickness are shown in Figure 26(d). Apparently, higher skin thickness will lead to a decrease of densification strain but significantly increase the plateau stress. This is the major reason for its high energy absorption capacity at higher thickness of skin.

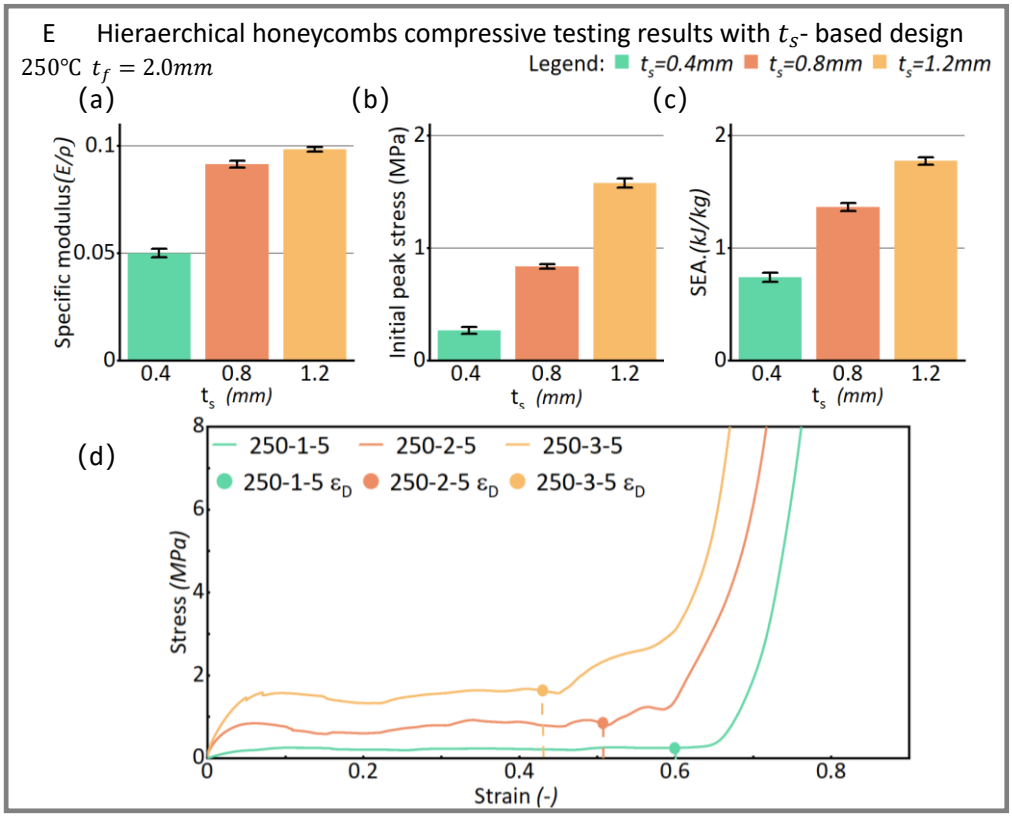

Figure 26 Results of hierarchical honeycomb structures with t_s ($t_s = 0.4, 0.8,$ and $1.2\,mm$) at 250℃ nozzle temperatures. (a) Specific modulus of hierarchical honeycomb structures with t_s ($t_s = 0.4, 0.8,$ and $1.2\,mm$) at 250℃nozzle temperatures; (b) Initial peak stress of hierarchical honeycomb structures with varying t_s ($t_s = 0.4, 0.8,$ and $1.2\,mm$) at 250℃nozzle temperatures; (c) Specific energy absorption (SEA.) of hierarchical honeycomb structures

with varying t_s ($t_s = 0.4, 0.8,$ and $1.2\,mm$) at 250℃ nozzle temperatures; (d) Strain-stress curves of hierarchical honeycomb structures with varying t_s ($t_s = 0.4, 0.8,$ and $1.2\,mm$) at 250℃ nozzle temperature and dotted lines indicate densification strain;

To compare the impact of increasing t_f and t_s on mechanical properties of hierarchical honeycomb structures, the relationship between relative density and the normalized elastic modulus E, initial peak stress σ_p, and the energy absorbed per unit volume W is fitted based on Ashby law for porous foaming materials [164][172] are summarized in Figure 27.

Compared to the design strategy of increasing core thickness (t_f), hierarchical honeycomb structures based on increasing skin thickness (t_s) exhibit worse performance (elastic modulus, initial peak stress and energy absorption) at the same relative density. It is evident that t_f-based hierarchical honeycomb structures surpass t_s-based designs in all performance metrics, including elastic modulus, initial peak stress, and energy absorption, at a relative density of approximately 13%.

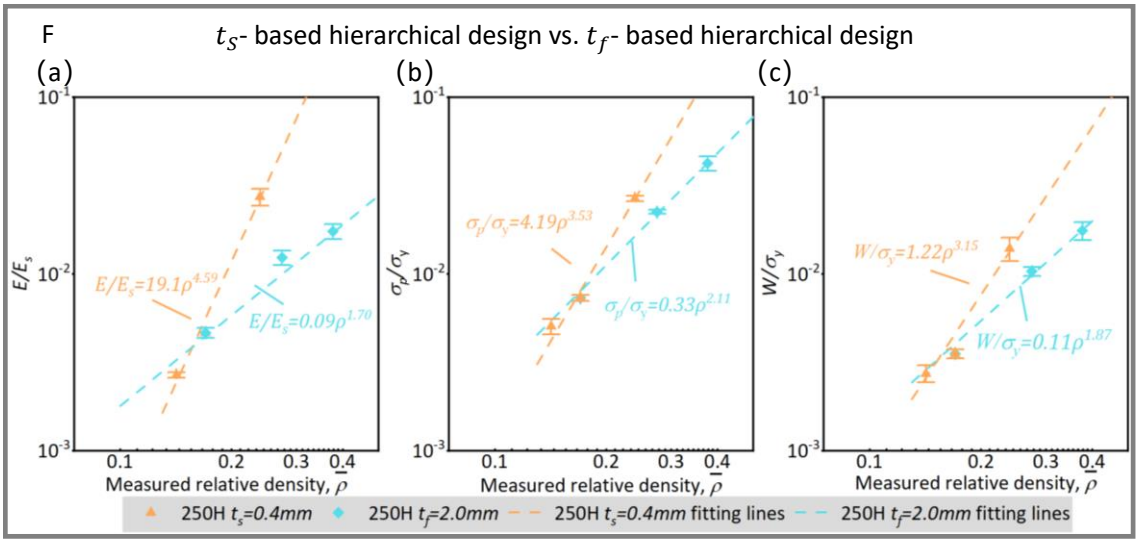

Figure 27 Normalized mechanical properties of hierarchical honeycomb tailoring with t_f and t_s along the in-plane direction with respect to the measured relative density: (a) elastic modulus, (b) initial peak stress, (c) energy per unit volume. Dashed lines indicate the best fitting lines of experimental data using power laws.

5.4.3 Design of honeycomb structures in energy absorption application

Figure 28 shows the summary of honeycomb structures fabricated under different process conditions and design

parameters. The horizontal axis is the density of fabricated honeycomb structures and vertical axis is the specific energy absorption. The dash line represents the iso-contour of energy absorption per unit volume. It is obvious that hierarchical honeycomb structures, and especially under 230℃ and 250℃ high nozzle temperatures, show their potential for energy absorption applications because of the high initial peak stress and high plateau stress, as highlighted in the previous section. Specifically, at high nozzle temperatures ($230°C$ and $250°C$), hierarchical honeycomb structures with skin thickness ($t_s = 3$) exhibited the highest energy absorption values ($651.3\,kJ$ and $656.6\,kJ$, respectively) in this research, while those with core thickness ($t_f = 10$) demonstrated the highest SEA values ($1.88\,kJ/kg$ and $2\,kJ/kg$, respectively). This suggests that the hierarchical honeycomb structures made by mixing Foaming PLA with PLA at a fabrication temperature of 250℃ with $t_s/t_f = 1/10$ exhibit the best performance in terms of SEA.

Based on the results of Figure 28, the following patterns can be summarized: Under low-density conditions, the limited wall thickness constrains the potential of hierarchical designs, resulting in solid PLA exhibiting superior energy absorption (EA) capabilities. However, under medium-to-high-density conditions, the increased wall thickness allows the potential of hierarchical designs to be realized, enabling hierarchical honeycomb structures to surpass solid PLA structures in both energy absorption (EA) and specific energy absorption (SEA). Moreover, a design method of hierarchical honeycomb structures for specific energy absorption could be described as follows (Details in **Appendix A**). Firstly, a diagram of 't_s or t_f vs. density' has been plotted. Then the relationship between thickness (t_s or t_f) and density could be described as linear. Next, we plot the figure of 'Density vs. specific energy absorption (SEA)', and their relationship has also been identified. Finally, the value of SEA (under nozzle temperature of 250℃) for t_s (SEA_{t_s}) and t_f (SEA_{t_f}) can be calculated using the equations: $SEA_{t_s} = -0.64{t_s}^2 + 2.84t_s - 1.3$ and $SEA_{t_f} = -0.45{t_f}^2 + 1.84t_f - 0.93$, where t_s denotes the thickness of PLA skins, and t_f denotes the thickness of foam PLA cores. Based on this method, the target properties on specific energy absorption can be controlled.

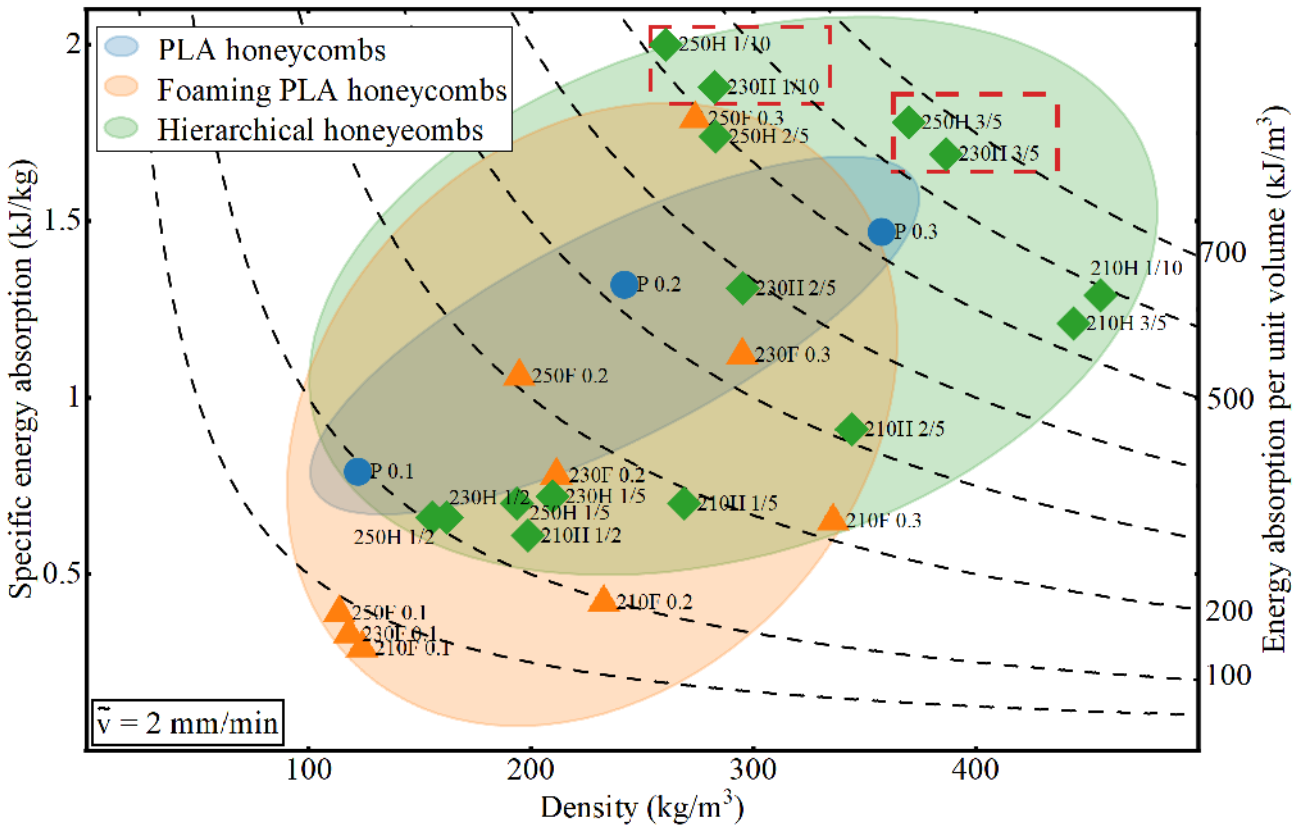

Figure 28 Energy absorption diagram of honeycomb structures in this research (Load speed $\tilde{V} = 2mm/min$).

Figure 29 shows a typical Ashby graph of specific energy absorption vs. density to compare energy absorption capacity of the proposed hierarchical honeycomb structures in the current study with polymer [173][176][177][178] and metallic [179][180][181] lattice structures with various cell geometries and architectures from literature. The single material lattices characteristically achieve specific energy absorption of $0.3-7.5\,kJ/kg$ within the density range of $17-800\,kg/m^3$. Specifically, within the given density range, the energy absorption of the hierarchical honeycomb structure is maintained at the same order of magnitude as that of stainless-steel lattice structures. Notably, the hierarchical honeycomb structure design proposed in this study elevates the energy absorption capacity of honeycomb structures to the level of metal lattice structures. With further optimization of the t_s, t_f, and nozzle temperature, the proposed hierarchical honeycomb structure design is expected to enhance its appeal in practical applications. Such adjustments will improve the mechanical performance and energy absorption capacity of the structure, offering a more competitive solution for engineering applications that demand both lightweight and high strength.

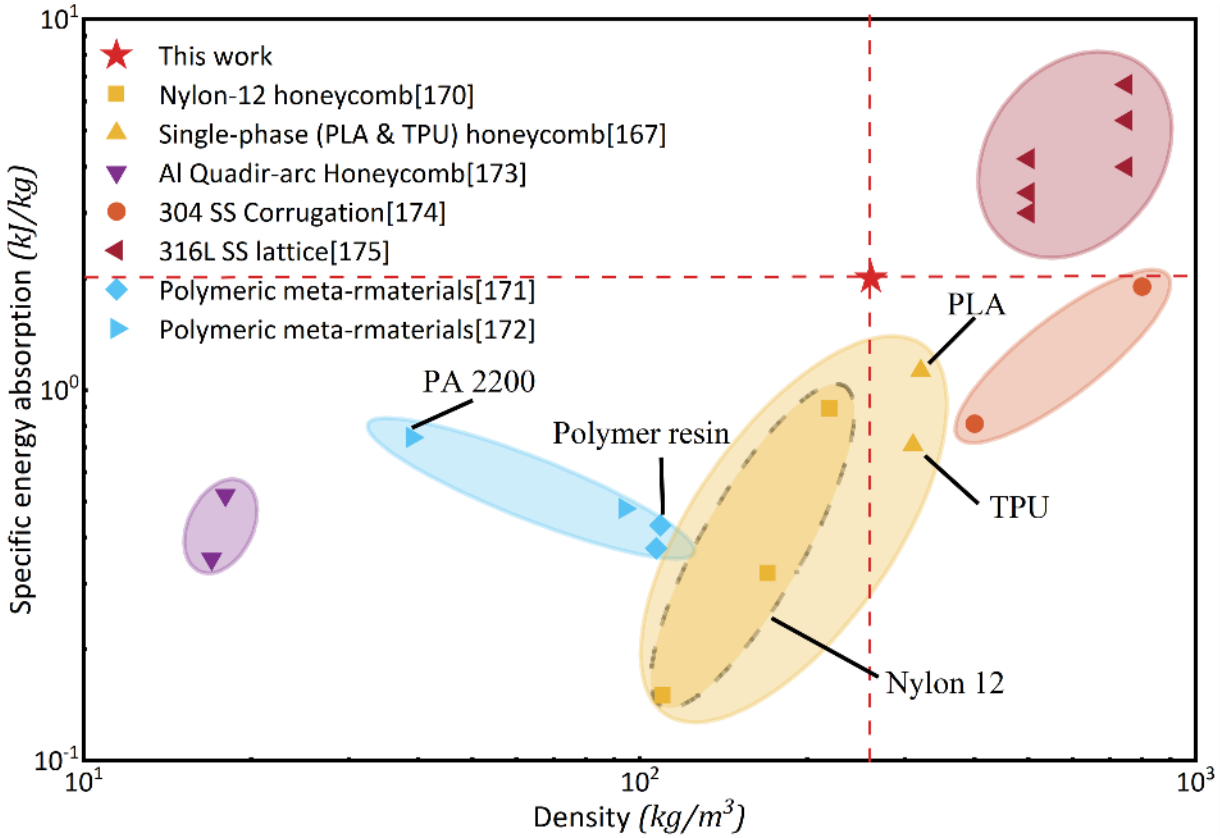

Figure 29 Ashby graph of specific energy absorption vs. density for the comparison of the energy absorption capacity of the proposed multi-material lattices in the current study with single-phase polymeric [173][176][177][178] and metallic [179][180][181] lattices with various cell geometries and architectures from the relevant literature.

5.5 Summary

This chapter presents a detailed experimental investigation into the mechanical properties of hierarchical honeycomb structures. The study focuses on how to design parameters, such as skin and core thickness, influence elastic modulus, initial peak stress, and energy absorption. Unidirectional compression tests were conducted following ASTM C365 to explore how these parameters can optimize structural performance. The following conclusions can be drawn Solid PLA exhibits a higher initial peak stress, while foaming PLA at high temperatures demonstrates excellent specific modulus and energy absorption capabilities. Its tunable mechanical properties with temperature changes reveal significant design potential. In the study of hierarchical honeycomb structures, t_f-based designs were found to surpass those of Solid PLA and foaming PLA on elastic modulus, initial peak stress and energy absorption at high relative densities. Furthermore,

after a relative density of 0.13, t_f-based designs consistently exhibit superior performance (elastic modulus, initial peaks stress and energy absorption) compared to t_s-based designs, further highlighting the advantages of increasing core thickness in enhancing mechanical properties.

Chapter 6: Conclusions and Future Research

The compressive responses of foaming PLA and PLA hierarchical honeycomb structures fabricated by FFF process are experimentally studied in this thesis. The compressive modulus, initial peak stress and energy absorption capabilities of three types of honeycomb structures (foaming PLA, solid PLA, and hierarchical honeycomb structures) are investigated and compared with different printing and design parameters (skin thickness t_s, foaming core thickness t_f , and nozzle temperatures). The major results from this research are summarized as follows:

1. **Stable and constant bead width achieved with fine-tuned flow parameters for foaming materials**: LSC model is developed to fine-tuning the flow multiplier for foaming materials printing. The printed results show the tuned flow multiplier can ensure accuracy and stable extrusion width across different nozzle temperatures ($210℃, 230℃,$ and $250℃$).

2. **Impacts of nozzle temperatures on physical and mechanical properties of foaming PLA materials**: Experiments on foaming materials with different nozzle temperatures have been done. Both SEM characterizations and uniaxial tension tests have been done on the printed foaming materials. The tensile results show both compressive elastic modulus and yield stress of foaming materials decrease with the increase of nozzle temperature. This is mainly due to the increase in pore size observed in the corresponding SEM images. However, the elongation does not follow the same trend. The maximum elongation has been achieved at 210 ℃, since it contains the small close-cell unit cell which usually exhibit higher elongation compared to open-cell foam. Thanks to its superior elongation performance, the PLA foaming materials at 210 ℃ can achieve higher tensile toughness than other samples including of solid PLA.

3. **Mechanical performance of honeycombs structures made of solid, foaming and hierarchical PLA materials:** In this research, the in-plane compressive performance of honeycomb structures made of solid, foaming and hierarchical PLA materials are investigated. The results show foaming PLA can achieve higher specific elastic modulus and specific energy absorption than its counterpart made of solid PLA, while solid PLA honeycomb has a slightly better initial peak stress which means it can sustain higher external loading. As to honeycomb structures made of hierarchical PLA materials, it shows that increasing the foaming core thickness, elastic modulus, initial

peak stress and energy absorption can be enhanced more efficiently than increasing the thickness of solid skin. In addition, a comparison has been made between honeycomb structures made of solid, foaming and hierarchical PLA materials, it shows the hierarchical honeycomb can achieve higher specific elastic modulus, peak stress and energy absorption capabilities during high overall relative density zone. This is due to the higher design freedom it provided to hierarchical honeycomb structures to redistribute materials between core and skin that can enhance the mechanical performance of structures. In general, the energy absorption capabilities of honeycomb structures with different base materials are summarized and compared. It is obviously foaming materials, and hierarchical structures significantly enlarge the material properties space of energy absorption capabilities. The honeycomb structures with hierarchical PLA printed under $250\ ℃$ nozzle temperature and $\frac{t_s}{t_f} = 1:10$ can achieve the highest specific energy absorption which is approximately 50% higher than the highest value for honeycomb structures made with traditional solid PLA materials. More importantly, this unique design provides unprecedent freedom for designers to further tailor the combination peak stress, energy absorption and relative density of honeycomb structures for specific requirements in different applications.

Although this research shows the promising future of honeycomb structures with hierarchical PLA, it still has certain limitations which can be further explored in the future.

First, it is necessary to extend this proposed approach to other base materials such as metal or composites structures which shows better stiffness and strength compared to polymer materials used in this research. By combining the material selection with structural design, it may further enhance the mechanical performance of designed hierarchical honeycomb structures.

Multiscale simulation models are also needed to help designers have a better prediction of honeycomb structures' performance. Even though honeycomb structures with hierarchical PLA materials enlarged design freedom, it also brings the challenge on efficiently exploring the material properties space. The multi-scale simulation model is needed to accelerate the exploration of materials' properties. Based on that, inverse design with the desired materials properties as input can be done.

References

[1]. Hattrick-Simpers, J., Li, K., Greenwood, M., Black, R., Witt, J., Kozdras, M., ... & Ozcan, O. (2023). Designing durable, sustainable, high-performance materials for clean energy infrastructure. Cell Reports Physical Science, 4(1).

[2]. Du Plessis, A., Razavi, N., Benedetti, M., Murchio, S., Leary, M., Watson, M., ... & Berto, F. (2022). Properties and applications of additively manufactured metallic cellular materials: A review. Progress in Materials Science, 125, 100918.

[3]. Jiang, W., Vlahopoulos, N., Castanier, M. P., Thyagarajan, R., & Mohammad, S. (2015). Tuning material and component properties to reduce weight and increase blastworthiness of a notional V-hull structure. Case Studies in Mechanical Systems and Signal Processing, 2, 19-28.

[4]. Rusch, K. C. (1970). Energy-absorbing characteristics of foamed polymers. Journal of Applied Polymer Science, 14(6), 1433-1447.

[5]. Fragoso-Medina, O., & Velázquez-Villegas, F. (2023). Aluminum foam to improve crash safety performance: a numerical simulation approach for the automotive industry. Mechanics Based Design of Structures and Machines, 51(7), 3583-3597.

[6]. Sidambe, A. T. (2014). Biocompatibility of advanced manufactured titanium implants—A review. Materials, 7(12), 8168-8188.

[7]. Iqbal, S., & Kamiński, M. (2024). Review Study on Mechanical Properties of Cellular Materials. Materials, 17(11), 2682.

[8]. Du Plessis, A., Razavi, N., Benedetti, M., Murchio, S., Leary, M., Watson, M., ... & Berto, F. (2022). Properties and applications of additively manufactured metallic cellular materials: A review. *Progress in Materials Science*, *125*, 100918.

[9]. Álvarez-Trejo, A., Cuan-Urquizo, E., Bhate, D., & Roman-Flores, A. (2023). Mechanical metamaterials with topologies based on curved elements: An overview of design, additive manufacturing and mechanical properties. *Materials & Design*, 112190.

[10]. Attarilar, S., Ebrahimi, M., Djavanroodi, F., Fu, Y., Wang, L., & Yang, J. (2021). 3D printing technologies in metallic implants: a thematic review on the techniques and procedures. *International Journal of Bioprinting*, *7*(1).

[11]. Zhakeyev, A., Wang, P., Zhang, L., Shu, W., Wang, H., & Xuan, J. (2017). Additive manufacturing: unlocking the evolution of energy materials. *Advanced Science*, *4*(10), 1700187.

[12]. Kaur, M., Han, S. M., & Kim, W. S. (2016). Three-dimensionally printed cellular architecture materials: perspectives on fabrication, material advances, and applications, MRS Commun. 7 (2016) 8–19.

[13]. Allegri, G., Yon, J., Hamerton, I., & Trask, R. S. A Route to Sustainable Aviation: A Roadmap for the Realization

of Aircraft Components with Electrical and Structural Multifunctionality.

[14]. Muhammad, A., Rahman, M. R., Baini, R., & Bakri, M. K. B. (2021). Applications of sustainable polymer composites in automobile and aerospace industry. In *Advances in sustainable polymer composites* (pp. 185-207). Woodhead Publishing.

[15]. Kamble, Z. (2023). Advanced structural and multi-functional sandwich composites with prismatic and foam cores: A review. *Polymer Composites*.

[16]. Chantarapanich, N., Laohaprapanon, A., Wisutmethangoon, S., Jiamwatthanachai, P., Chalermkarnnon, P., Sucharitpwatskul, S., ... & Sitthiseripratip, K. (2014). Fabrication of three-dimensional honeycomb structure for aeronautical applications using selective laser melting: a preliminary investigation. *Rapid Prototyping Journal*, *20*(6), 551-558.

[17]. Khan, S. A., Rahman, M. A., Khraisheh, M., & Hassan, I. G. (2024). Advances in 3D printed periodic lattice structures for energy research: Energy storage, transport and conversion applications.

[18]. Application of aluminum honeycomb panel on airplane (2021, 2 June) https://www.acebond.net/info/application-of-aluminum-honeycomb-panel-on-air-57918127.html

[19]. 7017 - 3D Pro Honeycomb Front Bumper (Option) (2019) https://www.rcmaker.com.au/products/7017-3d-pro-honeycomb-front-bumper-option

[20]. Six buildings that create a buzz with honeycomb-patterned facades (2018, 26 July) https://www.dezeen.com/2018/07/26/six-buildings-hexagon-pattern-honeycomb-facades/

[21]. High-Performance Basketball Knee Pads - Honeycomb Impact Protection (2019) https://www.temu.com/au/2pcs-basketball-knee-pads-honeycomb-anti-collision-sports-professional-training-knee-pads-for--mountaineering-g-601099544673274.html?refer_page_name=goods&refer_page_id=10032_1741602733702_m7w89q6tmx&refer_page_sn=10032&_x_sessn_id=bbqbymyn96

[22]. Solar Tile Technology Could Be 'Game Changer' For Clean Energy in Marine Sector (2021) https://www.maritimeindustries.org/news/solar-tile-technology-could-be-game-changer-clean-energy-marine-sector

[23]. Maconachie, T., Leary, M., Lozanovski, B., Zhang, X., Qian, M., Faruque, O., & Brandt, M. (2019). SLM lattice structures: Properties, performance, applications and challenges. Materials & Design, 183, 108137.

[24]. Bitzer, T. N. (1997). Honeycomb technology: materials, design, manufacturing, applications and testing. Springer Science & Business Media.

[25]. Lu, B., Li, D., & Tian, X. (2015). Development trends in additive manufacturing and 3D printing. Engineering, 1(1), 085-089.

[26]. Hoque, M. E., Chuan, Y. L., & Pashby, I. (2012). Extrusion based rapid prototyping technique: an advanced platform for tissue engineering scaffold fabrication. Biopolymers, 97(2), 83-93.

[27]. Fountain, J. E. (2004). Building the virtual state: Information technology and institutional change. Rowman & Littlefield.

[28]. Guzzi, E. A., & Tibbitt, M. W. (2020). Additive manufacturing of precision biomaterials. Advanced materials, 32(13), 1901994.

[29]. Schirmeister, C. G., Hees, T., Licht, E. H., & Mülhaupt, R. (2019). 3D printing of high density polyethylene by fused filament fabrication. Additive Manufacturing, 28, 152-159.

[30]. Banger, A., Jangid, N. K., Srivastava, A., & Srivastava, M. (2023). Polymeric Foams: Mechanisms and Properties. In Polymeric Foams: Fundamentals and Types of Foams (Volume 1) (pp. 43-61). American Chemical Society.

[31]. Wu, Y., Fang, J., Wu, C., Li, C., Sun, G., & Li, Q. (2023). Additively manufactured materials and structures: A state-of-the-art review on their mechanical characteristics and energy absorption. International Journal of Mechanical Sciences, 108102.

[32]. Jiang, J., Xu, X., & Stringer, J. (2019). Optimization of process planning for reducing material waste in extrusion based additive manufacturing. Robotics and Computer-Integrated Manufacturing, 59, 317-325.

[33]. Lukkassen, D., & Meidell, A. (2003). Advanced materials and structures and their fabrication processes. *Narrik University College, Hin*.

[34]. Pflug, J., Vangrimde, B., Verpoest, I., Bratfisch, P., & Vandepitte, D. (2003, May). Continuously produced honeycomb cores. In *INTERNATIONAL SAMPE SYMPOSIUM AND EXHIBITION* (pp. 602-611). SAMPE; 1999.

[35]. Murton, B. T. (2022). Methods for the creation of high performance cellular materials.

[36]. Kabir, S. F., Mathur, K., & Seyam, A. F. M. (2020). A critical review on 3D printed continuous fiber-reinforced composites: History, mechanism, materials and properties. *Composite Structures*, *232*, 111476.

[37]. Extrusion: A Manufacturing Process for Creating Various Shapes and Products (2021) https://www.richconn-cnc.com/what-is-extrusion.html

[38]. Pkg Knowledgebase http://pkgsolutions.co.uk/kb/Corrugating_Adhesives.php

[39]. Understanding the lamination of metal: Techniques and Benefit (2024, 27 August) https://blog.goldsupplier.com/lamination-of-metal/

[40]. Waldman, F. A. (1982). *The processing of microcellular foam* (Doctoral dissertation, Massachusetts Institute of Technology).

[41]. Coste, G., Negrell, C., & Caillol, S. (2020). From gas release to foam synthesis, the second breath of blowing agents. *European Polymer Journal*, *140*, 110029.

[42]. Calore, A. R., Srinivas, V., Groenendijk, L., Serafim, A., Stancu, I. C., Wilbers, A., ... & Moroni, L. (2023). Manufacturing of scaffolds with interconnected internal open porosity and surface roughness. *Acta Biomaterialia*, *156*, 158-176.

[43]. Ning, L., & Chen, X. (2017). A brief review of extrusion-based tissue scaffold bio-printing. *Biotechnology journal*, *12*(8), 1600671.

[44]. Yu, S., Bale, H., Park, S., Hwang, J. Y., & Hong, S. H. (2021). Anisotropic microstructure dependent mechanical behavior of 3D-printed basalt fiber-reinforced thermoplastic composites. *Composites Part B: Engineering*, *224*, 109184.

[45]. Rao, S., Jayaraman, K., & Bhattacharyya, D. (2011). Short fibre reinforced cores and their sandwich panels: Processing and evaluation. *Composites Part A: Applied Science and Manufacturing*, *42*(9), 1236-1246.

[46]. Zaharia, S. M., Enescu, L. A., & Pop, M. A. (2020). Mechanical performances of lightweight sandwich structures produced by material extrusion-based additive manufacturing. *Polymers*, *12*(8), 1740.

[47]. Ongaro, F. (2018). Estimation of the effective properties of two-dimensional cellular materials: a review. *Theoretical and Applied Mechanics Letters*, *8*(4), 209-230.

[48]. Xu, Z., Razavi, S. M. J., & Ayatollahi, M. R. (2022). 00019 Functionally Graded Lattice Structures: Fabrication Methods, Mechanical Properties, Failure Mechanisms and Applications. *International Journal of Impact Engineering*, *125*, 163-172.

[49]. KanagaMadhuraN, H. D., Sneha, J., Gnanavel, G., & Prabhu, N. (2019). Review on Manufacturing of Cellular Polymers and Its Applications. *IOSR Journal of Polymer and Textile Engineering*, *6*(5), 9-22.

[50]. Ansari, A. I., & Sheikh, N. A. (2023). A review on different approaches for foam fabrication. *Journal of The Institution of Engineers (India): Series C*, *104*(6), 1219-1245.

[51]. Tofail, S. A., Koumoulos, E. P., Bandyopadhyay, A., Bose, S., O'Donoghue, L., & Charitidis, C. (2018). Additive manufacturing: scientific and technological challenges, market uptake and opportunities. *Materials today*, *21*(1), 22-37.

[52]. Khan, N., & Riccio, A. (2024). A systematic review of design for additive manufacturing of aerospace lattice structures: Current trends and future directions. *Progress in Aerospace Sciences*, *149*, 101021.

[53]. Zhang, Q., Shi, Y., & Zhao, Z. (2022). A brief review of mechanical designs for additive manufactured soft materials. *Soft Sci*, *2*(2).

[54]. Ren, L., Wang, Z., Ren, L., Han, Z., Liu, Q., & Song, Z. (2022). Graded biological materials and additive manufacturing technologies for producing bioinspired graded materials: An overview. *Composites Part B: Engineering*, *242*, 110086.

[55]. Bhat, C., Prajapati, M. J., Kumar, A., & Jeng, J. Y. (2024). Additive Manufacturing-Enabled Advanced Design and Process Strategies for Multi-Functional Lattice Structures. *Materials*, *17*(14), 3398.

[56]. Nazir, A., Gokcekaya, O., Billah, K. M. M., Ertugrul, O., Jiang, J., Sun, J., & Hussain, S. (2023). Multi-material additive manufacturing: A systematic review of design, properties, applications, challenges, and 3D printing of materials and cellular metamaterials. *Materials & Design*, *226*, 111661.

[57]. Wang, Y., Zhang, L., Daynes, S., Zhang, H., Feih, S., & Wang, M. Y. (2018). Design of graded lattice structure with

optimized mesostructures for additive manufacturing. Materials & Design, 142, 114-123.

[58]. Schmelzle, J., Kline, E. V., Dickman, C. J., Reutzel, E. W., Jones, G., & Simpson, T. W. (2015). (Re) Designing for part consolidation: Understanding the challenges of metal additive manufacturing. Journal of Mechanical Design, 137(11), 111404.

[59]. Li, S., Xin, Y., Yu, Y., & Wang, Y. (2021). Design for additive manufacturing from a force-flow perspective. Materials & Design, 204, 109664.

[60]. Nouri, A., Shirvan, A. R., Li, Y., & Wen, C. (2021). Additive manufacturing of metallic and polymeric load-bearing biomaterials using laser powder bed fusion: A review. Journal of Materials Science & Technology, 94, 196-215.

[61]. Rajendra Boopathy, V., & Sriraman, A. (2019). Energy absorbing capability of additive manufactured multi-material honeycomb structure. Rapid Prototyping Journal, 25(3), 623-629.

[62]. Gleadall, A. (2021). FullControl GCode Designer: open-source software for unconstrained design in additive manufacturing. *Additive Manufacturing*, *46*, 102109.

[63]. Chen, L. Y., Liang, S. X., Liu, Y., & Zhang, L. C. (2021). Additive manufacturing of metallic lattice structures: Unconstrained design, accurate fabrication, fascinated performances, and challenges. Materials Science and Engineering: R: Reports, 146, 100648.

[64]. Li, Y., Feng, Z., Hao, L., Huang, L., Xin, C., Wang, Y., ... & Peijs, T. (2020). A review on functionally graded materials and structures via additive manufacturing: from multi-scale design to versatile functional properties. Advanced Materials Technologies, 5(6), 1900981.

[65]. Liu, G., Zhang, X., Chen, X., He, Y., Cheng, L., Huo, M., ... & Lu, J. (2021). Additive manufacturing of structural materials. Materials Science and Engineering: R: Reports, 145, 100596.

[66]. Jiang, J., Xu, X., & Stringer, J. (2018). Support structures for additive manufacturing: a review. Journal of Manufacturing and Materials Processing, 2(4), 64.

[67]. Walter, A., & Marcham, C. L. (2020). Environmental advantages in additive manufacturing. Professional Safety, 65(01), 34-38.

[68]. Surjadi, J. U., Gao, L., Du, H., Li, X., Xiong, X., Fang, N. X., & Lu, Y. (2019). Mechanical metamaterials and their engineering applications. Advanced Engineering Materials, 21(3), 1800864.

[69]. Xiao, L., Xu, X., Feng, G., Li, S., Song, W., & Jiang, Z. (2022). Compressive performance and energy absorption of additively manufactured metallic hybrid lattice structures. International Journal of Mechanical Sciences, 219, 107093.

[70]. Grima, J. N., Gatt, R., Ravirala, N., Alderson, A., & Evans, K. E. (2006). Negative Poisson's ratios in cellular foam materials. Materials Science and Engineering: A, 423(1-2), 214-218.

[71]. Schaedler, T. A., & Carter, W. B. (2016). Architected cellular materials. Annual Review of Materials Research, 46,

187-210.

[72]. Sun, Y., & Li, Q. M. (2018). Dynamic compressive behaviour of cellular materials: A review of phenomenon, mechanism and modelling. International Journal of Impact Engineering, 112, 74-115.

[73]. Zhang, J., Li, D., & Wang, M. (2024). Multi-material fused deposition modelling of structural–functional integrated absorber with multi-scale structure possessing tunable broadband microwave absorption. Materials & Design, 246, 113315.

[74]. Gilchrist, C. L., Ruch, D. S., Little, D., & Guilak, F. (2014). Micro-scale and meso-scale architectural cues cooperate and compete to direct aligned tissue formation. Biomaterials, 35(38), 10015-10024.

[75]. Ranut, P., Nobile, E., & Mancini, L. (2014, April). Microtomography-based CFD analysis of transport in open-cell aluminum metal foams. In Journal of Physics: Conference Series (Vol. 501, No. 1, p. 012021). IOP Publishing.

[76]. European Space Agency – ESA (1970, 1 January). Rapid prototype of honeycomb structure. https://demideity-semideaf-parapegma.click/?u=tpap60a&o=zlbwly0&cid=0f5ef1d7-67a1-4a20-bf4e-7099895307ec

[77]. EikoSim (2019, 2 December). Digital Image Correlation for lattice structures. https://eikosim.com/en/use-cases/digital-image-correlation-lattice-structures/?print=print

[78]. Nofar, M., Utz, J., Geis, N., Altstädt, V., & Ruckdäschel, H. (2022). Foam 3D printing of thermoplastics: a symbiosis of additive manufacturing and foaming technology. Advanced Science, 9(11), 2105701.

[79]. Dilberoglu, U. M., Gharehpapagh, B., Yaman, U., & Dolen, M. (2017). The role of additive manufacturing in the era of industry 4.0. Procedia manufacturing, 11, 545-554.

[80]. Huang, Y., Leu, M. C., Mazumder, J., & Donmez, A. (2015). Additive manufacturing: current state, future potential, gaps and needs, and recommendations. Journal of Manufacturing Science and Engineering, 137(1), 014001.

[81]. Hegab, H., Khanna, N., Monib, N., & Salem, A. (2023). Design for sustainable additive manufacturing: A review. Sustainable Materials and Technologies, e00576.

[82]. Li, D., Liao, W., Dai, N., & Xie, Y. M. (2019). Comparison of mechanical properties and energy absorption of sheet-based and strut-based gyroid cellular materials with graded densities. Materials, 12(13), 2183.

[83]. Bhate, D., Penick, C. A., Ferry, L. A., & Lee, C. (2019). Classification and selection of cellular materials in mechanical design: Engineering and biomimetic approaches. Designs, 3(1), 19.

[84]. Vasvári, G., Haimhoffer, Á., Horváth, L., Budai, I., Trencsényi, G., Béresová, M., ... & Fenyvesi, F. (2019). Development and characterisation of gastroretentive solid dosage form based on melt foaming. AAPS PharmSciTech, 20, 1-11.

[85]. Banhart, J. (2001). Manufacture, characterisation and application of cellular metals and metal foams. Progress in materials science, 46(6), 559-632.

[86]. Prabhu, S., Raja, V. B., & Nikhil, R. (2015). Applications of cellular materials–an overview. Applied Mechanics and Materials, 766, 511-517.

[87]. Jiang, C., Wang, J., Wallner, J., & Pottmann, H. (2014, August). Freeform honeycomb structures. In Computer Graphics Forum (Vol. 33, No. 5, pp. 185-194).

[88]. Ngo, T. D., Kashani, A., Imbalzano, G., Nguyen, K. T., & Hui, D. (2018). Additive manufacturing (3D printing): A review of materials, methods, applications and challenges. Composites Part B: Engineering, 143, 172-196.

[89]. Turner, B. N., Strong, R., & Gold, S. A. (2014). A review of melt extrusion additive manufacturing processes: I. Process design and modeling. Rapid prototyping journal, 20(3), 192-204.

[90]. Galgalikar, R. (2012). Design automation and optimization of honeycomb structures for maximum sound transmission loss.

[91]. de Formanoir, C., Suard, M., Dendievel, R., Martin, G., & Godet, S. (2016). Improving the mechanical efficiency of electron beam melted titanium lattice structures by chemical etching. Additive Manufacturing, 11, 71-76.

[92]. Ngo, T. D., Kashani, A., Imbalzano, G., Nguyen, K. T., & Hui, D. (2018). Additive manufacturing (3D printing): A review of materials, methods, applications and challenges. Composites Part B: Engineering, 143, 172-196.

[93]. Bracconi, M., Ambrosetti, M., Maestri, M., Groppi, G., & Tronconi, E. (2018). A fundamental analysis of the influence of the geometrical properties on the effective thermal conductivity of open-cell foams. Chemical Engineering and Processing-Process Intensification, 129, 181-189.

[94]. Mills, N. J. (2007). The high strain mechanical response of the wet Kelvin model for open-cell foams. International Journal of solids and structures, 44(1), 51-65.

[95]. Drobny, J. G. (2014). Handbook of thermoplastic elastomers. Elsevier.

[96]. Amin, K. F., & Rashed, H. M. (2019). Steel used in construction industries.

[97]. Li, D., Liao, W., Dai, N., & Xie, Y. M. (2019). Comparison of mechanical properties and energy absorption of sheet-based and strut-based gyroid cellular materials with graded densities. Materials, 12(13), 2183.

[98]. Zhou, H., Zhao, M., Ma, Z., Zhang, D. Z., & Fu, G. (2020). Sheet and network based functionally graded lattice structures manufactured by selective laser melting: Design, mechanical properties, and simulation. International Journal of Mechanical Sciences, 175, 105480.

[99]. Benedetti, M., Du Plessis, A., Ritchie, R. O., Dallago, M., Razavi, S. M. J., & Berto, F. (2021). Architected cellular materials: A review on their mechanical properties towards fatigue-tolerant design and fabrication. Materials Science and Engineering: R: Reports, 144, 100606.

[100]. Du Plessis, A., Razavi, S. M. J., Benedetti, M., Murchio, S., Leary, M., Watson, M., ... & Berto, F. (2022). Properties and applications of additively manufactured metallic cellular materials: A review. Progress in Materials Science, 125, 100918.

[101]. Megson, T. H. G. (2019). Structural and stress analysis. Butterworth-Heinemann.

[102]. Yang, E., Leary, M., Lozanovski, B., Downing, D., Mazur, M., Sarker, A., ... & Brandt, M. (2019). Effect of geometry on the mechanical properties of Ti-6Al-4V Gyroid structures fabricated via SLM: A numerical

study. Materials & Design, 184, 108165.

[103]. Hu, X. U. (2021). Additively manufactured lead zirconate titanate–polymer composites with sheet-based triply periodic minimal surface structures (Doctoral dissertation, RMIT University).

[104]. Zou, S., Mu, Y., Pan, B., Li, G., Shao, L., Du, J., & Jin, Y. (2022). Mechanical and biological properties of enhanced porous scaffolds based on triply periodic minimal surfaces. Materials & Design, 219, 110803.

[105]. Li, K., Gao, X. L., & Wang, J. (2007). Dynamic crushing behavior of honeycomb structures with irregular cell shapes and non-uniform cell wall thickness. International Journal of Solids and Structures, 44(14-15), 5003-5026.

[106]. Zhang, Q., Yang, X., Li, P., Huang, G., Feng, S., Shen, C., ... & Lu, T. J. (2015). Bioinspired engineering of honeycomb structure–Using nature to inspire human innovation. Progress in Materials Science, 74, 332-400.

[107]. Zhang, Q., Yang, X., Li, P., Huang, G., Feng, S., Shen, C., ... & Lu, T. J. (2015). Bioinspired engineering of honeycomb structure–Using nature to inspire human innovation. Progress in Materials Science, 74, 332-400.

[108]. Gong, X., Liu, L., Scarpa, F., Leng, J., & Liu, Y. (2017). Variable stiffness corrugated composite structure with shape memory polymer for morphing skin applications. Smart Materials and Structures, 26(3), 035052.

[109]. Tripathi, L., & Behera, B. K. (2021). 3D woven honeycomb composites. Journal of Materials Science, 56, 15609-15652.

[110]. Lee, S. T., & Park, C. B. (Eds.). (2014). Foam extrusion: principles and practice. CRC press.

[111]. Ries, S., Spörrer, A., & Altstädt, V. (2014, May). Foam injection molding of thermoplastic elastomers: Blowing agents, foaming process and characterization of structural foams. In AIP Conference Proceedings (Vol. 1593, No. 1, pp. 401-410). American Institute of Physics.

[112]. Times News Service (2023, 04 January). PDO weighs massive 3D printing of oilfield spare parts with French technology. https://timesofoman.com/article/125191-pdo-weighs-massive-3d-printing-of-oilfield-spare-parts-with-french-technology

[113]. Bioplastics News Logo (2014, 15 February). Bioplastic and 3D Printing. https://bioplasticsnews.com/2014/02/15/bioplastics-and-3d-printing/

[114]. Tom van Eekelen (2022, 19 April). Prevent excessive build plate distortion in additive manufacturing. https://blogs.sw.siemens.com/simcenter/prevent-excessive-build-plate-distortion-in-additive-manufacturing/

[115]. Yang, J., Yang, D., Tao, Y., & Shi, J. (2024). Machine learning assisted prediction and analysis of in-plane elastic modulus of hybrid hierarchical square honeycombs. Thin-Walled Structures, 198, 111736. Sunkara, V. (2013). MS Thesis, Texas A&M University.

[116]. Rusch, K. C. (1970). Energy-absorbing characteristics of foamed polymers. Journal of Applied Polymer Science, 14(6), 1433-1447.Sunkara, V. (2013). MS Thesis, Texas A&M University.

[117]. Fragoso-Medina, O., & Velázquez-Villegas, F. (2023). Aluminum foam to improve crash safety performance: a numerical simulation approach for the automotive industry. Mechanics Based Design of Structures and

Machines, 51(7), 3583-3597.Akhmetshin, L., et al. (2023). Designs, 7(6), 129.

[118]. Sidambe, A. T. (2014). Biocompatibility of advanced manufactured titanium implants—A review. Materials, 7(12), 8168-8188.

[119]. Iqbal, S., & Kamiński, M. (2024). Review Study on Mechanical Properties of Cellular Materials. Materials, 17(11), 2682.

[120]. Caccese, V., Ferguson, J. R., & Edgecomb, M. A. (2013). Optimal design of Honeycomb structure used to mitigate head impact. Composite structures, 100, 404-412.

[121]. Panda, B., Leite, M., Biswal, B. B., Niu, X., & Garg, A. (2018). Experimental and numerical modelling of mechanical properties of 3D printed honeycomb structures. Measurement, 116, 495-506.

[122]. Yang, Y., Liu, H., Zhang, Q., Ma, J., Yang, X., & Yang, J. (2023). Energy absorption characteristics of a super hexagonal honeycomb under out-of-plane crushing. Thin-Walled Structures, 189, 110914. Zhu, J., et al. (2021). Materials & Design, 198, 109312.

[123]. Benedetti, M., et al. (2021). Architected cellular materials: A review on their mechanical properties towards fatigue-tolerant design and fabrication. Materials Science and Engineering: R: Reports, 144, 100606.

[124]. Abueidda, D. W., et al. (2017). Mechanical properties of 3D printed polymeric cellular materials with triply periodic minimal surface architectures. Materials & Design, 122, 255-267.

[125]. Yang, L., et al. (2019). Continuous graded Gyroid cellular materials fabricated by selective laser melting: Design, manufacturing and mechanical properties. Materials & Design, 162, 394-404.

[126]. Du Plessis, A., et al. (2022). Properties and applications of additively manufactured metallic cellular materials: A review. Additive Manufacturing, 58, 103007.

[127]. Rashed, M. G., et al. (2016). Metallic microlattice materials: A current state of the art on manufacturing, mechanical properties and applications. Materials & Design, 95, 518-533.

[128]. Qi, C., et al. (2021). Advanced honeycomb designs for improving mechanical properties: A review. Composite Structures, 262, 113640.

[129]. Zhang, X., et al. (2020). Modelling and characterization of mechanical properties of optimized honeycomb structure. Materials & Design, 192, 108747.

[130]. Panda, B., et al. (2018). Experimental and numerical modelling of mechanical properties of 3D printed honeycomb structures. Measurement, 116, 495-506.

[131]. Ingrole, A., et al. (2017). Design and modeling of auxetic and hybrid honeycomb structures for in-plane property enhancement. Materials & Design, 117, 72-83.

[132]. Chen, X., & Fu, Q. (2018). Design and modeling of a combined embedded enhanced honeycomb with tunable mechanical properties. Materials & Design, 141, 116-125.

[133]. Ma, N., Han, S., Xu, W., Han, Q., & Li, C. (2024). Compressive response and optimization design of a novel hierarchical re-entrant origami honeycomb metastructure. Engineering Structures, 306, 117819.

[134]. Huang, W., Zhang, Y., Su, L., Liu, B., Li, K., & Zhang, F. (2022). A bi-factorial hierarchical honeycomb with promising crushing resistance. International Journal of Mechanical Sciences, 229, 107511.

[135]. Usta, F., Scarpa, F., & Türkmen, H. S. (2020). Edgewise compression of novel hexagonal hierarchical and asymmetric unit cells honeycomb metamaterials. Materials Today Communications, 24, 101102.

[136]. Sun, Y., & Pugno, N. M. (2013). In plane stiffness of multifunctional hierarchical honeycombs with negative Poisson's ratio sub-structures. Composite Structures, 106, 681-689.

[137]. Taylor, C. M., Smith, C. W., Miller, W., & Evans, K. E. (2011). The effects of hierarchy on the in-plane elastic properties of honeycombs. International Journal of Solids and Structures, 48(9), 1330-1339.

[138]. Qin, R., Wang, X., Lu, J., Li, Q., Niu, H., Zhang, X., & Chen, B. (2024). Node-locked multi-cell honeycomb for efficient energy absorption. International Journal of Mechanical Sciences, 268, 109028.

[139]. Chen, Z., Li, J., Wu, B., Chen, X., & Xie, Y. M. (2024). Enhanced mechanical properties of re-entrant auxetic honeycomb with self-similar inclusion. Composite Structures, 331, 117921.

[140]. Tao, Y., Li, W., Cheng, T., Wang, Z., Chen, L., Pei, Y., & Fang, D. (2021). Out-of-plane dynamic crushing behavior of joint-based hierarchical honeycombs. Journal of Sandwich Structures & Materials, 23(7), 2832-2855.

[141]. Hu, D., Wang, Y., Song, B., Dang, L., & Zhang, Z. (2019). Energy-absorption characteristics of a bionic honeycomb tubular nested structure inspired by bamboo under axial crushing. Composites Part B: Engineering, 162, 21-32.

[142]. He, Q., Feng, J., & Zhou, H. (2019). A numerical study on the in-plane dynamic crushing of self-similar hierarchical honeycombs. Mechanics of Materials, 138, 103151.

[143]. Kafle, A., Luis, E., Silwal, R., Pan, H. M., Shrestha, P. L., & Bastola, A. K. (2021). 3D/4D Printing of polymers: Fused deposition modelling (FDM), selective laser sintering (SLS), and stereolithography (SLA). Polymers, 13(18), 3101.

[144]. Chen, Y., Wang, N., Ola, O., Xia, Y., & Zhu, Y. (2021). Porous ceramics: Light in weight but heavy in energy and environment technologies. Materials Science and Engineering: R: Reports, 143, 100589.

[145]. Feldman, D. (2010). Polymeric foam materials for insulation in buildings. In Materials for Energy Efficiency and Thermal Comfort in Buildings (pp. 257-273). Woodhead Publishing.

[146]. Guanghong, H., & Yue, W. (2012). Microcellular foam injection molding process. Some critical issues for injection molding, 175-202.

[147]. Zuo, Z. H., Huang, X., Rong, J. H., & Xie, Y. M. (2013). Multi-scale design of composite materials and structures for maximum natural frequencies. Materials & Design, 51, 1023-1034.

[148]. Coelho, P. G., Guedes, J. M., & Cardoso, J. B. (2019). Topology optimization of cellular materials with

periodic microstructure under stress constraints. Structural and Multidisciplinary Optimization, 59, 633-645.

[149]. Benedetti, M., Du Plessis, A., Ritchie, R. O., Dallago, M., Razavi, S. M. J., & Berto, F. (2021). Architected cellular materials: A review on their mechanical properties towards fatigue-tolerant design and fabrication. Materials Science and Engineering: R: Reports, 144, 100606.

[150]. Langrand, B., Casadei, F., Marcadon, V., Portemont, G., & Kruch, S. (2017). Experimental and finite element analysis of cellular materials under large compaction levels. International Journal of Solids and Structures, 128, 99-116.

[151]. Al-Saedi, D. S., Masood, S. H., Faizan-Ur-Rab, M., Alomarah, A., & Ponnusamy, P. (2018). Mechanical properties and energy absorption capability of functionally graded F2BCC lattice fabricated by SLM. Materials & Design, 144, 32-44.

[152]. Vigliotti, A., & Pasini, D. (2012). Stiffness and strength of tridimensional periodic lattices. Computer methods in applied mechanics and engineering, 229, 27-43.

[153]. Ashby, M. F. (2006). The properties of foams and lattices. Philosophical Transactions of the Royal Society A: Mathematical, Physical and Engineering Sciences, 364(1838), 15-30.

[154]. Austermann, J., Redmann, A. J., Dahmen, V., Quintanilla, A. L., Mecham, S. J., & Osswald, T. A. (2019). Fiber-reinforced composite sandwich structures by co-curing with additive manufactured epoxy lattices. Journal of Composites Science, 3(2), 53.

[155]. Wu, Y., & Yang, L. (2020). The effect of unit cell size and topology on tensile failure behavior of 2D lattice structures. International Journal of Mechanical Sciences, 170, 105342.

[156]. Benedetti, M., Du Plessis, A., Ritchie, R. O., Dallago, M., Razavi, S. M. J., & Berto, F. (2021). Architected cellular materials: A review on their mechanical properties towards fatigue-tolerant design and fabrication. Materials Science and Engineering: R: Reports, 144, 100606.

[157]. Stamenović, D., & Wang, N. (2011). Stress transmission within the cell. Comprehensive Physiology, 1(1), 499.

[158]. Maconachie, T., Leary, M., Zhang, J., Medvedev, A., Sarker, A., Ruan, D., ... & Brandt, M. (2020). Effect of build orientation on the quasi-static and dynamic response of SLM AlSi10Mg. Materials Science and Engineering: A, 788, 139445.

[159]. Nofar, M., Utz, J., Geis, N., Altstädt, V., & Ruckdäschel, H. (2022). Foam 3D printing of thermoplastics: A symbiosis of additive manufacturing and foaming technology. Advanced Science, 9(11), 2105701.

[160]. M. Li, J. Jiang, B. Hu, W. Zhai, Compos. Sci. Technol. 2020, 200, 108454;

[161]. Dave, H. K., Rajpurohit, S. R., Patadiya, N. H., Dave, S. J., Sharma, K. S., Thambad, S. S., ... & Sheth, K. V. (2019). Compressive strength of PLA based scaffolds: effect of layer height, infill density and print speed. Int. J. Mod. Manuf. Technol, 11(1), 21-27.

[162]. Zenkert, D., & Burman, M. (2009). Tension, compression and shear fatigue of a closed cell polymer

foam. Composites Science and Technology, 69(6), 785-792.

[163]. Gupta, N., Ye, R., & Porfiri, M. (2010). Comparison of tensile and compressive characteristics of vinyl ester/glass microballoon syntactic foams. Composites Part B: Engineering, 41(3), 236-245.

[164]. Gibson, L. J. (2003). Cellular solids. Mrs Bulletin, 28(4), 270-274.

[165]. Li, D., Qin, R., Xu, J., Zhou, J., & Chen, B. (2022). Improving mechanical properties and energy absorption of additive manufacturing lattice structure by struts' node strengthening. Acta Mechanica Solida Sinica, 35(6), 1004-1020.

[166]. Rajak, D. K., Gupta, M., Rajak, D. K., & Gupta, M. (2020). Materials Selection and Design Considerations. An Insight Into Metal Based Foams: Processing, Properties and Applications, 53-80.

[167]. Q. Li, I. Magkiriadis, J.J. Harrigan, Compressive strain at the onset of densification of cellular solids, J. Cell. Plast. 42 (5) (2006) 371–392.

[168]. Maskery, N. Aboulkhair, A. Aremu, C. Tuck, I. Ashcroft, R.D. Wildman, R.J. Hague, A mechanical property evaluation of graded density Al-Si10-Mg lattice structures manufactured by selective laser melting, Mater. Sci. Eng. A 670 (2016) 264–274.

[169]. Al Hassanieh, S., Alhantoobi, A., Khan, K. A., & Khan, M. A. (2021). Mechanical properties and energy absorption characteristics of additively manufactured lightweight novel re-entrant plate-based lattice structures. Polymers, 13(22), 3882.

[170]. Liu, R., Chen, W., & Zhao, J. (2024). A review on factors affecting the mechanical properties of additively-manufactured lattice structures. Journal of Materials Engineering and Performance, 33(10), 4685-4711.

[171]. Malek, S., & Gibson, L. (2015). Effective elastic properties of periodic hexagonal honeycombs. Mechanics of Materials, 91, 226-240.

[172]. Meza, L. R., Phlipot, G. P., Portela, C. M., Maggi, A., Montemayor, L. C., Comella, A., ... & Greer, J. R. (2017). Reexamining the mechanical property space of three-dimensional lattice architectures. Acta Materialia, 140, 424-432.

[173]. Yavas, D., Liu, Q., Zhang, Z., & Wu, D. (2022). Design and fabrication of architected multi-material lattices with tunable stiffness, strength, and energy absorption. Materials & Design, 217, 110613.

[174]. Maiti, S. K., Gibson, L. J., & Ashby, M. F. (1984). Deformation and energy absorption diagrams for cellular solids. Acta metallurgica, 32(11), 1963-1975.

[175]. Ridlwan, M., Nurgesang, F. A., Riza, R., & Syafi'i, N. M. (2022). Mechanical properties of sandwich composite using glass fiber reinforced polymer as a skin and 3D printed polylactic acid as a core. Journal of Mechanical Engineering, Science, and Innovation, 2(1), 44-54.

[176]. Habib, F. N., Iovenitti, P., Masood, S. H., & Nikzad, M. (2017). In-plane energy absorption evaluation of 3D printed polymeric honeycombs. Virtual and Physical Prototyping, 12(2), 117-131.

[177]. Mohsenizadeh, M., Gasbarri, F., Munther, M., Beheshti, A., & Davami, K. (2018). Additively-manufactured lightweight Metamaterials for energy absorption. Materials & Design, 139, 521-530.

[178]. Chen, X., Ji, Q., Wei, J., Tan, H., Yu, J., Zhang, P., ... & Kadic, M. (2020). Light-weight shell-lattice metamaterials for mechanical shock absorption. International Journal of Mechanical Sciences, 169, 105288.

[179]. Zhang, D., Fei, Q., & Zhang, P. (2017). In–plane dynamic crushing behavior and energy absorption of honeycombs with a novel type of multi-cells. Thin-Walled Structures, 117, 199-210.

[180]. Han, B., Yan, L. L., Yu, B., Zhang, Q. C., Chen, C. Q., & Lu, T. J. (2014). Collapse mechanisms of metallic sandwich structures with aluminum foam-filled corrugated cores. J. Mech. Mater. Struct, 9(4), 397-425.

[181]. Cao, X., Duan, S., Liang, J., Wen, W., & Fang, D. (2018). Mechanical properties of an improved 3D-printed rhombic dodecahedron stainless steel lattice structure of variable cross section. International Journal of Mechanical Sciences, 145, 53-63.

Appendix A

Taking the t_s or t_f – based design under $250℃$ as example. The relationship between thickness (t_s or t_f – based design) vs. density is shown in Figure 30(a). And the relationship between density and specific energy absorption is shown in Figure 30(b).

The relationship between thickness and density can be described as follows:

$$\rho_{t_s} = 110.13t_s + 105.93 \quad (1)$$

$$\rho_{t_f} = 32.87t_f + 128.74 \quad (2)$$

Where ρ_{t_s} denotes the density of hierarchical based on t_s design, t_s denotes the thickness controlled by adjusting the solid PLA skins, ρ_{t_f} denotes the density of hierarchical based on t_f design, and t_f denotes the thickness controlled by adjusting the foam PLA cores.

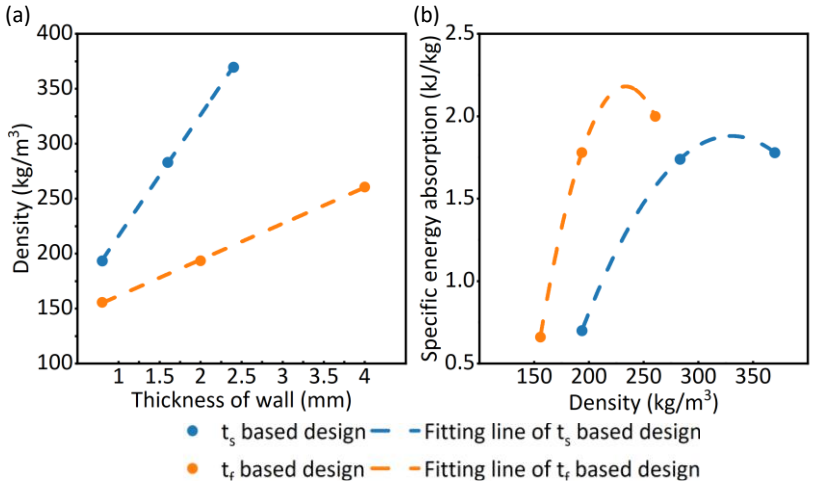

Figure 30 (a) Diagram of thickness (t_s or t_f – based design) vs. Density; (b) Diagram of Density vs. Specific energy absorption.

And the relationship between density and specific energy absorption is identified:

$$SEA_{t_s} = -6.33 \times 10^{-5} {\rho_{t_s}}^2 + 0.042\rho_{t_s} - 5.022 \quad (3)$$

$$SEA_{t_f} = -2.49 \times 10^{-4} {\rho_{t_f}}^2 + 0.116\rho_{t_f} - 11.443 \quad (4)$$

Where SEA_{t_s} denotes the specific energy absorption value of t_s – based design hierarchical honeycombs, and SEA_{t_f} denotes the specific energy absorption value of t_f – based design hierarchical honeycombs.

To analyze the dependency of thickness and SEA value, the expression for ρ_{t_s} and ρ_{t_f} derived in Eq. (1) and (2) is substituted into Eq. (3) and (4), leading to a reformulated representation of Eq. (3) and (4), followed by normalization to ensure consistency in the resulting equation:

$$SEA_{t_s} = -0.63527{t_s}^2 + 2.8443t_s - 1.3024 \quad (5)$$

$$SEA_{t_f} = -0.44561{t_f}^2 + 1.8443t_f - 0.9352 \quad (6)$$